Niksoney Azevedo Mendonça, Juliana Aljahara, Victor Souza Silva, Thaís Elias Almeida

https://doi.org/10.1590/SciELOPreprints.15500

Submetido em: 2026-03-17
Postado em: 2026-03-20 (versão 1)
(AAAA-MM-DD)

A multidimensional view of fronds reveals phenotypic structuring and delimitation problems

Niksoney Azevedo Mendonça[1*], Juliana Aljahara[1], D. Victor Souza e Silva[1] & Thaís Elias Almeida[1]

[1]Programa de Pós-graduação em Biologia Vegetal, Centro de Biociências, Universidade Federal de Pernambuco, Recife–PE, Av. Professor Moraes Rego, 1235, 50670-420, Brazil.

Short title:

A multidimensional view of fronds

Orcid:

NAM - https://orcid.org/0000-0002-5336-011X

JA - https://orcid.org/0000-0001-9852-6622

DVSS - https://orcid.org/0009-0003-1885-6616

TEA - https://orcid.org/0000-0002-1611-1333

Keywords:

Elliptical Fourier Analysis; Evolution; Integrative Taxonomy; *Microgramma*; Near Infrared Spectroscopy; Outline Morphometry; Phylogenetic Signal.

ABSTRACT

- Recognizing lineages is a central challenge in plant systematics, making it essential to explore multiple analytical tools. In this context, this study investigates how frond shape can assist in discriminating against lineages within the Scaly clade of *Microgramma* (Polypodiaceae), and tests whether the integration of multiple lines of evidence enables a more consistent recognition of lineages than exclusively macromorphological approaches.
- We analyzed 271 specimens representing eight species, using Elliptical Fourier Analysis (EFA) to quantify frond shape, followed by multivariate statistical tests (PCA, MANOVA, LDA). Evolutionary relationships between spectral and morphometric data were assessed through phylogenetic generalized least squares (PGLS) regressions and phylogenetic partial least squares (Phylo-PLS) analyses.
- Dimorphic species exhibited higher discrimination capacity (average accuracy of 80–83%). Fertile and combined fronds yielded the highest accuracy values. Morphologically similar species, such as *M. reptans* and *M. tobagensis*, showed significant overlap, whereas *M. percussa* achieved the best performance (average accuracy of 80%). Morphometric-spectral integration showed a strong correlation ($R^2 = 0.72$; $P = 0.003$), and both the combined datasets (spectra and outline) and the individual datasets of spectral and shape features revealed a high phylogenetic signal (λ = 1–0.84), indicating partial coevolution between frond shape, chemical composition, and the evolutionary history of the group.
- Outline morphometry combined with infrared spectroscopy within a phylogenetic framework improves lineage discrimination, although overlap zones persist, reflecting complex evolutionary processes. Our study highlights the potential of integrative systematics to elucidate species boundaries in groups with high morphological disparity, as well as the need for broad sampling and multi-evidence approaches in future systematic reviews.

INTRODUCTION

Species delimitation remains a central challenge in systematics, as the boundaries between lineages are frequently obscured by evolutionary factors such as hybridization and introgression (Taylor & Larson 2019), incomplete lineage sorting (Pease *et al.* 2018), phenotypic plasticity (Forsman 2015), and incipient speciation (Roux *et al.* 2016), which generate patterns of genotypic and phenotypic variation, hindering the recognition of discrete units (Dayrat 2005; Wiens 2007; Padial *et al.* 2010). In many cases, these processes give rise to species complexes, groups where the number of taxa and their boundaries remain uncertain (Pinheiro *et al.* 2018). As a consequence, morphological delimitation is frequently challenged both by cryptic species that consist of genetically divergent but morphologically similar lineages (Bickford *et al.* 2007; Struck *et al.* 2018) and by the opposite scenario, in which high intraspecific variation within a single lineage produces morphotypes that simulate the existence of multiple taxonomic entities (Dayrat 2005; Padial *et al.* 2010).

Historically, taxonomy has primarily relied on qualitative assessments of macromorphological characters, which often result in problematic and poorly reproducible species circumscriptions (Dayrat 2005; Wiens 2007; André & Almeida 2025). Although the traditional morphological approach has been fundamental for the initial organization of biodiversity, its limitations in dealing with phenotypic plasticity, homoplasy, convergence, and morphological overlap have frequently produced species circumscriptions inconsistent with the evolutionary history of lineages (Schlick-Steiner *et al.* 2010; Padial *et al.* 2010). In this context, integrative taxonomy has emerged as a necessary alternative, treating species not as fixed entities but as evolutionary hypotheses to be tested through multiple lines of evidence (Dayrat 2005; De Queiroz 2007; Schlick-Steiner *et al.* 2010; Padial *et al.* 2010). This approach explores different dimensions of organismal diversity, allowing for more stable and evolutionarily meaningful delimitations (Pante *et al.* 2015; Karbstein *et al.* 2024).

Species delimitation is particularly challenging in some taxonomic groups, such as ferns. The combination of few diagnostic morphological characters, extensive homoplasy, polyploidy, and recurrent hybridization hampers the precise definition of species (Haufler *et al.* 2000; Schneider *et al.* 2009; Wood *et al.* 2009; Almeida *et al.* 2021; Mondal & Moktan 2022). Furthermore, fern taxonomy has historically focused almost exclusively on the sporophyte, neglecting the gametophyte, a crucial stage in the life cycle of these plants (Krieg & Chambers 2022). This partial perspective generates significant gaps in our understanding of fern evolutionary history and diversity patterns (Kessler & Aros-Mualin 2025). Given these gaps, the use of quantitative and multidimensional phenotypic descriptors that go beyond traditional qualitative observation is essential.

Microgramma C.Presl (Polypodiaceae) comprises approximately thirty predominantly neotropical, epiphytic species (Almeida 2014; Almeida *et al.* 2021). Characterized by high morphological disparity, including frond dimorphism, the genus is taxonomically challenging due to homoplasy, overlapping traits, and possible hybridization events (Almeida 2014; Almeida *et al.* 2021). The Scaly clade includes eight species with contrasting biogeographic patterns, ranging from widespread and disjunct distributions to cases of microendemism (Lima *et al.* in press). The group comprises both dimorphic (*M. nana* (Liebm.) T.E.Almeida*, M. reptans* (Cav.) A.R.Sm.*, M. tecta* (Kaulf.) Alston*, M. tobagensis* (C.Chr.) C.D.Adams & Baksh.-Com.) and monomorphic species, (*M. dictyophylla* (Kunze ex Mett.) de la Sota*, M. latevagans* (Maxon & C.Chr.) Lellinger, *M. percussa* (Cav.) de la Sota*, M. piloselloides* (L.) Copel.). However, several morphological characters overlap among species, and high levels of homoplasy complicate species delimitation (Almeida 2014; Almeida *et al.* 2021).

Given that the Scaly clade is fully sampled in phylogenetic studies and includes four dimorphic and four monomorphic species with distributions ranging from wide to more restricted, it constitutes an ideal model for testing integrative approaches. In this sense, this study aims to

address two main questions: (I) Is frond shape structured within lineages and informative for distinguishing these species hypotheses? and (II) Do morphological and spectral phenotypic data corroborate species hypotheses in a phylogenetic context?

MATERIALS AND METHODS

Sampling processing, and data analysis

We selected 271 specimens from different herbaria, representing all eight species of the Scaly clade (Table S1). We used the species concepts of Almeida (2014, 2026) and Almeida *et al.* (2021) as premises for testing. Specimens were chosen to capture the species' geographic distribution and intraspecific morphological variation, following Almeida (2014, 2026). All identifications were reviewed and confirmed by the first and last authors. Data from outline-based geometric morphometrics and spectral readings were each divided into three datasets for each species: (I) sterile fronds, (II) fertile fronds, and (III) sterile and fertile fronds combined. All analyses were performed in the R environment (R Core Team 2025).

Frond shape variation analyses

Frond shape variation was quantified through Outline-based Geometric Morphometrics and analyzed using Elliptical Fourier Analysis (EFA) (Fig. S1). Images of dried specimens were extracted from online repositories, including GBIF (Global Biodiversity Information Facility, https://www.gbif.org/) and SpeciesLink (https://specieslink.net/), from which sterile and fertile fronds were isolated and repositioned separately per specimen on a uniform white background using GIMP v. 2.10.38 (https://www.gimp.org/). After isolation, 2D shape coordinates (x, y) were obtained using the DiaOutline software (Wishkerman & Hamilton 2018). Unlike other tools, DiaOutline handles issues related to contour starting points, as tracing proceeds from left to right; however, all images must share a consistent orientation (Wishkerman & Hamilton 2018). Extracted coordinates were imported, processed, and

analyzed using the *momocs* package (Bonhomme *et al.* 2014). To determine the optimal number of harmonics contributing to the cumulative harmonic power in the EFA, we tested configurations ranging from six to ten harmonics using Leave-One-Out Cross-Validation (LOOCV) (Table 1). In the analysis, each specimen was successively removed from the dataset and used as a test unit, while the remaining specimens were used to train the classification model (Hastie *et al.* 2009). After the model was fitted with the training set, we used it to predict the taxonomic identity of the removed specimen; this was repeated until all specimens were used once as a test unit (Hastie *et al.* 2009). Based on this, the ideal number of harmonics was chosen based on overall classification accuracy and the balance among predicted classes (species performance). The selected configurations were six harmonics for dataset I (sterile fronds), seven harmonics for dataset II (fertile fronds), and nine harmonics for dataset III (combined fronds; Table 1). Principal Component Analysis (PCA) was applied to the Fourier coefficients to reduce data dimensionality and explore outline shape variation, identifying the main components contributing to morphological differentiation (Greenacre *et al.* 2022). A Multivariate Analysis of Variance (MANOVA) was then conducted using the principal components derived from the Fourier coefficients to test significant differences among classes and datasets. This statistical framework allows the simultaneous evaluation of multiple dependent variables (Denis 2020). In this case, the principal axes of morphological variation are relative to a categorical factor, enabling the detection of morphological differences among tested hypotheses (Denis 2020). Additionally, Linear Discriminant Analysis (LDA) was performed using the mean frond values per specimen as analytical units (Liu 2013). This approach avoids pseudo-replication from multiple fronds per individual, ensuring observation independence. LDA, a supervised technique, distinguishes and classifies groups by projecting features from a higher-dimensional space into a lower-dimensional one, facilitating efficient separation among classes (Liu 2013).

149 **Spectral signature**

150 To identify the most informative spectral bands across sterile, fertile, and combined datasets,
151 we applied the minimum-redundancy–maximum-relevance (mRMR) band selection method
152 (Ma *et al.* 2024) implemented in the *mRMRe* package. This technique maximizes the relevance
153 of spectral bands with respect to the variable response while minimizing redundancy among
154 them (Ma *et al.* 2024). The optimal number of spectral bands was determined using the
155 geometric elbow criterion applied to the R^2 (coefficient of determination) values of ranked
156 bands (Satopää *et al.* 2011). The inflection point was defined as the band exhibiting the highest
157 perpendicular distance from the line connecting the first and last bands in the R^2 × ranking
158 plot (Fig. S2). Following the methods described in Mendonça *et al.* (2026), spectral data were
159 acquired using a PerkinElmer Frontier™ near-infrared Fourier transform spectrometer (FT-
160 NIR) available at (https://github.com/labevofern/Microgramma-FTNIR).

161 **Phylogenetic comparative analyses**

162 To provide a phylogenetic framework for comparative morphometric and spectral analyses,
163 we used the pruned version of the *Microgramma* chloroplast phylogenetic inference from
164 Mendonça *et al.* (2026). This tree was based on the Bayesian phylogenetic tree published by
165 Almeida *et al.* (2021).

166 Phylogenetic Generalized Least Squares (PGLS) analyses were employed to assess the
167 phylogenetic influence on outline and spectral variation, separately for each dataset
168 (Felsenstein 1985; Martins & Hansen 1997). This approach tests evolutionary hypotheses for
169 continuous traits by assessing whether model residuals follow a specific evolutionary model,
170 thus correcting for phylogenetic non-independence (Revell 2010). Tree manipulation and
171 PGLS modeling were performed using the packages *ape* (Paradis & Schliep 2019) for general
172 phylogenetic operations and *caper* (Orme *et al.* 2025) to run PGLS models via the 'pgls()'
173 function. For each of the six datasets (sterile fronds spectra, sterile fronds outlines, fertile

fronds spectra, fertile fronds outlines, combined fronds spectra, and combined fronds outlines), principal component (PC) scores were obtained from PCA, and the first two PC axes were used. The phylogenetic scaling parameter λ (Pagel 1999) was estimated for each model by maximum likelihood (λ = "ML"), while the evolutionary parameters κ (kappa) and δ (delta) were fixed at 1.0, assuming a standard Brownian motion model for the rate of phenotypic evolution.

To test the hypothesis of coevolution between frond shape and spectral signatures, we evaluated the integration between these two modules using Phylogenetic Partial Least Squares (Phylo-PLS) analysis (Adams & Felice 2014; Mittelheiser 2022; Casadei-Ferreira *et al.* 2024). This method quantifies the correlation between datasets while statistically controlling for shared evolutionary history (Adams & Felice 2014; Adams & Collyer 2018). Input data consisted of the first two PC scores for the fronds outline shape and spectral signature. Phylo-PLS was implemented using a phylogenetically independent contrasts approach (Felsenstein 1985). PCA scores were standardized (mean = 0, SD = 1) using the 'scale()' function implemented in base R (R Core Team 2025). The phylogenetic variance–covariance (VCV) matrix was computed using 'vcv.phylo()' from the *ape* package, and standardized data were transformed into phylogenetically independent contrasts by pre-multiplying them by the square root of the inverse VCV matrix. Subsequently, Partial Least Squares regression was performed on the phylogenetic contrasts using the 'plsr()' function from the *pls* package (Mevik & Wehrens 2007). The *phytools* (Revell 2012) and *geiger* (Pennell *et al.* 2014) packages supported data and phylogenetic tree manipulation.

RESULTS

General patterns of frond shape variation

The PCA of sterile fronds showed that the first two axes accounted for 95.1% of the total shape

variation (PCA1 = 92.4% and PCA2 = 2.7%; Fig. 2A). Considerable overlap occurred among several species. However, *Microgramma nana* occupied a relatively distinct morphospace, partially overlapping with individuals of *M. tecta*, *M. piloselloides*, and *M. reptans* (Fig. 2A). Overall, sterile fronds showed less morphospace overlap than either fertile or combined fronds.

For fertile fronds (Fig. 2B), the first two PCA axes accounted for 88.5% of shape variation (PCA1 = 65.9% and PCA2 = 22.6%; Fig. 2B). Species of the Scaly clade overlapped extensively in morphospace, whereas *Microgramma latevagans* was the only species showing a markedly distinct position, as indicated by the distance of its centroid (larger circles; Fig. 2B).

In the PCA including the combined dataset of both fronds (Fig. 2C), the first two axes explained 95.5% of shape variation (PCA1 = 92.2% and PCA2 = 3.3%; Fig. 2C). Species exhibited more evident overlap, although some consistent patterns were detected. Sterile and fertile fronds of dimorphic species (*M. nana*, *M. reptans*, *M. tecta*, and *M. tobagensis*) occupied distinct regions of the morphospace (Fig. 2C). In monomorphic species (*M. dictyophylla*, *M. latevagans*, *M. percussa*, and *M. piloselloides*), sterile and fertile fronds overlapped in the multidimensional space (Fig. 2C).

When the PCA was performed considering only dimorphism and monomorphism, the first two axes explained 95.5% of the variation (PCA1 = 92.25% and PCA2 = 3.31%; Fig. S3). Although there was extensive overlap, the dispersion of dimorphic species within the multidimensional space was greater compared to monomorphic species (Fig. S3A).

Morphological delimitation and classification performance between species

The Linear Discriminant Analysis (LDA) (Fig. 3A–C) and corresponding confusion matrices (Fig. 3D–F) revealed that the fertile frond dataset had the most accurate predictions. For sterile fronds, the first two LDA axes explained 89.5% of the total variation (LDA1 = 75.4% and

LDA2 = 14.1%; Table 1, Fig. 3A,D). Groupings formed relatively distinct clusters, although considerable overlap persisted among some species. The corresponding confusion matrix (Table 1, Fig. 3D) showed uneven classification performance across groups. The highest accurate classifications were recorded for *M. dictyophylla* (70%), *M. nana* (74%), and *M. reptans* (73%; Table 1, Fig. 3D). Conversely, *M. latevagans* (25%) and *M. tobagensis* (69%) Table 1, Fig. 3D) showed lower accuracy. Misclassification was particularly frequent for *M. percussa*, with 32% of its individuals reassigned to *M. dictyophylla*, followed by *M. latevagans* with 31% misclassifications as *M. piloselloides*, and *M. tobagensis* showed 25% misclassifications with *M. reptans* (Fig. 3D).

For fertile fronds, the first two LDA axes explained 90.9% of shape variation (LDA1 = 55.4% and LDA2 = 35.5%; Table 1, Fig. 3B,E). The polygons had less overlap than those from sterile fronds (Fig. 3B). This improvement was reflected in higher accuracy in the confusion matrix (Table 1, Fig. 3E). Classification performance was solid for *M. latevagans* and *M. percussa* (88% each), and robust for *M. reptans* (76%) and *M. dictyophylla* (71%) (Fig. 3E). *Microgramma nana* showed 42% accuracy and showed considerable overlap, particularly with *M. tecta*, as 32% of *M. nana* individuals were classified as *M. tecta* (Fig. 3E).

In the combined dataset, the first two LDA axes explained 87.2% of the shape variation (LDA1 = 73.4% and LDA2 = 13.8%; Table 1, Fig. 3C,F). This analysis revealed an intermediate pattern between the previous two datasets, both in group delimitation and classification performance (Fig. 3C,F). The highest accuracy value was again found for *M. percussa* (85%), followed by *M. reptans* (82%) and *M. piloselloides* (79%), suggesting that these species exhibit relatively better morphological patterns when combined, or even better for sterile fronds in the case of *M. percussa* (Table 1, Fig. 3C). In contrast, *M. dictyophylla* (60%) and *M. tobagensis* (62%) had lower performance, with higher misclassification rates associated with *M. percussa* (33%) and *M. reptans* (68%; Table 1, Fig. 3C). *Microgramma nana* (71%)

showed improved accuracy when compared with the fertile-only dataset, but still showed relevant errors, particularly with *M. tecta* (23%) (Table 1, Fig. 3C). *Microgramma tecta* showed the lowest accuracy overall, exhibiting strong overlap with other taxa (Table 1, Fig. 3C).

In the LDA comparing dimorphic versus monomorphic groups, the discriminant variable LD1 showed an asymmetric distribution between the two categories (Fig. S3B). Dimorphic species were concentrated in negative LD1 values, whereas monomorphic species predominated in positive values, with limited overlap between distributions. Classification accuracy reached 83% for dimorphic and 78% for monomorphic species, indicating sufficient morphological discrimination between these groups (Table 1).

Morphological differences among species groups

The Multivariate Analysis of Variance (MANOVA) revealed consistent and statistically significant morphological differences in the datasets (sterile, fertile, and combined), both in sterile and fertile contexts, as well as in the combined analysis (Table S2, Fig. S4). In sterile fronds (Fig. S4A), a strong pattern of morphological segregation was evident, with most pairwise comparisons showing highly significant differences ($P < 0.001$). Only the contrast between *M. reptans* and *M. latevagans* yielded a marginally significant result ($P < 0.1$). In fertile fronds (Fig. S4B), morphological differentiation was even stronger: in addition to most comparisons remaining highly significant ($P < 0.001$), several additional contrasts reached moderate ($P < 0.05$) or strong ($P < 0.01$) significance. In the combined analysis (Fig. S4C), the overall pattern of significant distinction among species persisted, with predominantly highly significant values ($P < 0.001$). Mean shapes derived from pairwise PCA comparisons (Fig. S4D–F) visually illustrate the nature of these morphological differences. In sterile fronds (Fig. S4D), deformation ellipses highlight outline and length–width ratio variations that characterize certain groups, albeit at smaller magnitudes. In fertile fronds (Fig. S4E),

differences likely associated with reproductive structures (sporangia on the abaxial surface) accentuate changes in margin shape, symmetry, and, in some cases, lamina elongation, producing clearly distinct mean profiles, particularly between dimorphic and monomorphic species. In the combined analysis (Fig. S4F), these patterns remain consistent, supporting the existence of distinguishable mean shapes among species.

Association among outlines, spectral traits, and evolutionary history

The Phylogenetic Generalized Least Squares (PGLS) analysis applied to spectral and outline data combined revealed distinct association patterns between the first two principal components (PC1 and PC2), depending on the dataset (Fig. 4, Table S3). In sterile frond spectra, results indicated no significant relationship between principal components (R^2 = 0.023; P = 0.721). Pagel's λ was equal to zero, indicating the absence of phylogenetic signal (Fig. 4A, Table S3). Similarly, sterile frond shape showed no phylogenetic structure or significant association (R^2 = 0.001; P = 0.982; λ = 0) (Fig. 4B, Table S3). In fertile fronds, spectral data also revealed no significant phylogenetic signal (R^2 = 0; P = 0.962; λ = 0) (Fig. 4B, Table S3). In contrast, fertile frond shape exhibited a moderate phylogenetic signal (R^2 = 0.243; P = 0.215; λ = 0.888). Although not statistically significant, the relatively high λ suggests a moderate evolutionary association, implying that fertile frond morphology may partially reflect phylogenetic patterns among species (Fig. 4E, Table S3).

When considering combined datasets (sterile+fertile fronds), the explanatory power of both spectral and morphometric data increased. The combined spectral dataset yielded R^2 = 0.299 (P = 0.160; λ = 1), indicating a strong phylogenetic signal and a considerable proportion of explained variance despite the lack of conventional significance (Fig. 4C, Table S3). Similarly, the combined frond shape produced R^2 = 0.303 (P = 0.157; λ = 0.843), reinforcing that integrating sterile and fertile fronds captures evolutionary patterns in both shape and spectral domains (Fig. 4D, Table S3).

299 **Integration between outline and spectral attributes**

300 The Phylogenetic Partial Least Squares (Phylo-PLS) analysis revealed consistent patterns of
301 integration between frond shape (Shape PCs) and spectral properties (Spectra PCs) in
302 *Microgramma* species (Fig. 5, Fig. S5). When all datasets were combined, including sterile
303 and fertile fronds (Fig. 5A, Fig. S5), a strong and significant association was observed (R^2 =
304 0.72; P = 0.003). In this set, Comp1 showed a high loading for Spectra PC2 (0.975) and Shape
305 PC2 (0.834), while Shape PC1 also contributed positively (0.598) and presented the highest
306 relative importance value (VIP = 1.269; Table S4). In Comp2, Shape PC1 showed the highest
307 loading in modulus (−0.923), followed by Spectra PC2 (0.794), indicating that the covariation
308 between shape and spectra is strongly structured by these axes when all specimens are
309 considered (Table S4).
310 In the sterile set (Fig. 5, Fig. S5), the integration remained significant (R^2 = 0.57; P = 0.025).
311 Comp1 had the greatest contribution from Shape PC1 (−0.857; VIP = 1.008) and Spectra_PC1
312 (0.690), followed by Spectra PC2 (0.567) and Shape PC2 (0.549; VIP = 0.991; Table S4).
313 Comp2 showed the greatest contribution from Shape PC2 (0.729) and Shape PC1 (0.685),
314 reflecting the predominance of morphometric variation in this axis (Table S4). In the fertile
315 set, the association between shape and spectra was weaker and not significant (R^2 = 0.24; P =
316 0.166; Fig. 5B, Fig. S5). Comp1 had high and positive loadings for Shape PC1 (0.745; VIP =
317 1.007) and Shape PC2 (0.673; VIP = 0.993), while the spectral axes exhibited lower values
318 (Spectra PC1 = 0.170; Spectra PC2 = 0.038; Table S4). In Comp2, Shape PC1 and Shape PC2
319 showed opposite loadings (−0.733 and 0.680, respectively), maintaining a reduced
320 participation of the spectral variables (Table S4).
321 The phylogenetic structure of the variation is depicted in Fig. 5D, showing that PLS1 scores
322 are not randomly distributed among species. The dendrogram indicates that closely related
323 species share similar integration patterns with more pronounced deviations in certain taxa

(Fig. 5D). Morphologically, *M. latevagans* and *M. dictyophylla* showed extreme values in the combined dataset, while in the spectral domain, *M. latevagans* and *M. piloselloides* stood out, especially in fertile fronds (Fig. 5D). The heatmaps further illustrate this heterogeneity: shape variation was more evenly distributed across species, whereas spectral diversity was concentrated in a subset of taxa, indicating higher spectral differentiation (Fig. 5D).

DISCUSSION

Our results demonstrate that the integration of outline morphometrics with near-infrared spectroscopy provides robust discrimination of fern lineages. Despite considerable variation in frond shape and areas of overlap (Fig. 2), predictive models using a multi-evidence approach reveal that shape and spectra evolved in an integrated manner. The combination of sterile and fertile fronds optimized their diagnostic value (Fig. 5).

The variation in frond shape observed in the Scaly clade, as evidenced by Principal Component Analysis (PCA; Fig. 2), showed significant overlap between lineages in morphospace. When evaluating the frond datasets separately (sterile, fertile, and combined), sterile fronds showed slightly less overlap in morphospace, while fertile fronds and the combined set exhibited more pronounced overlaps. The exception was fertile fronds of *M. latevagans*, which presented a centroid further away from the other overlapping lineages (Fig. 2b). However, discriminant analyses (LDA) revealed that, despite this visual continuity, frond shape carries a strong diagnostic signal for some lineages. Models based on isolated fertile fronds and the combined set (sterile + fertile) provided greater discrimination capacity and overall predictive accuracy than sterile fronds alone (Fig. 3). These results are supported by statistically significant outline differences (MANOVA) between species in all scenarios (Fig. S2). Despite its effectiveness, this methodology has not yet been widely used in ferns; it was first applied by Morilla *et al.* (2017), who evaluated the variation in frond shape within the

Nephrolepidaceae and Thelypteridaceae families. In their work, Elliptic Fourier Analysis (EFA) and multivariate analyses revealed subtle shape-related differences, highlighting both intraspecific and interspecific variation. Comparable approaches have been successfully applied to other plant lineages to validate morphological hypotheses and investigate variation based on frond outline geometry (*e.g.*, Viscosi & Fortini 2011; Adebowale *et al.* 2012; Nascimento *et al.* 2021; Gaem *et al.* 2022). As observed in our results, these studies demonstrate that, even in areas of strong overlap, quantitative analyses can reveal gradual transitions consistent with species boundaries (Viscosi & Fortini 2011; Speed & Arbuckle 2016; Reginato & Michelangeli 2016).

Despite the overall discriminatory capacity observed, when we deepened the evaluation of multivariate performance for the species individually, the accuracy varied and revealed ecological and taxonomic dynamics. For example, *M. dictyophylla* and *M. percussa* showed high rates of cross-misclassification, with 32% of *M. percussa* individuals being incorrectly designated in the sterile frond model (Table 1, Fig. 3). However, despite being close in the morphospace, they exhibit clear signs of individuality that are combined with other characteristics not captured by the contour, such as rhizome scale morphology and paraphyse density (Almeida 2014, 2026). This distinction is corroborated by near-infrared spectroscopy (FT-NIR) data, in which *M. percussa* achieved 100% and *M. dictyophylla* obtained more than 90% predictive accuracy. This indicates that the species possess highly distinct and diagnosable chemical and morphological signatures, even though the general shape of the frond overlaps (Mendonça *et al.* 2026).

Similar dynamics of outline overlap counterbalanced by subtle morphological differences or geographical separation were evident in other species pairs: *Microgramma nana* and *M. tecta*, *M. latevagans* and *M. piloselloides*, and *M. reptans* and *M. tobagensis* (Almeida 2014; Lima *et al.* 2025) Previously considered a variety of *M. tecta* (*M. tecta* var. *nana* (Liebm.) Mickel

& Beitel; Mickel & Beitel 1988), its taxonomic distinction from *M. tecta* uses the shape of the blade scales and paraphyses (Almeida 2014, 2026). Although morphologically similar, these species occur allopatrically and show little niche overlap (Lima *et al.* 2025). According to Mendonça *et al.* (2026), the spectral predictive accuracy (average of 83% for *M. tecta* and 81% for *M. nana*) and identification error rates may reflect morphological similarities, including frond size and abaxial surface indument, which can mask the spectral signal of the fronds (Almeida *et al.* 2021; Mendonça *et al.* 2026).

Microgramma latevagans and *M. piloselloides*, while morphologically close, can be distinguished by their allopatric geographic ranges and several diagnostic traits. *Microgramma latevagans* is restricted to the Andes, while *M. piloselloides* occurs widely in Central America and the Caribbean (Lima *et al.* 2025). Additionally, the sterile frond apex is acuminate in *M. latevagans* versus rounded to rarely acute in *M. piloselloides*, and differences in rhizome and frond indument are also present between the species (Almeida 2014). Spectral analysis corroborates the distinction between these lineages, demonstrating that *M. latevagans* and *M. piloselloides* are recovered as distinct spectral entities. The confusion matrix of spectral data revealed clear segregation between the two species (Mendonça *et al.* 2026). Only one recorded cross was limited to a single sterile specimen of *M. latevagans* erroneously identified as *M. piloselloides*, reinforcing that the geographic isolation and evolutionary individuality of *M. latevagans* are reflected in a diagnostic spectral signature (Mendonça et al. 2026).

On the other hand, the morphological affinity between *M. reptans* and *M. tobagensis*, previously highlighted by Almeida (2014), was confirmed by our analyses (Table 1, Fig. 2). These species share very similar sterile fronds, characterized by thin venation and overlapping forms, which historically made it difficult to identify specimens without fertile fronds (Almeida 2014). The most evident morphological characteristic that differentiates the species

is the presence of sori that project beyond the fertile frond margin in *M. reptans*, visible on the adaxial surface (Almeida 2014, 2026). This strong phenotypic overlap is directly reflected in the FT-NIR spectral models, which showed evident cross-prediction errors between these two taxa (*M. tobagensis* specimens incorrectly classified as *M. reptans* and vice versa; Mendonça *et al.* 2026). This congruence between morphometric and spectral ambiguity highlights the complexity of species delimitation in this group. This challenge is further reflected in the phylogenetic relationships that suggest the polyphyly of *M. tobagensis* (Almeida *et al.* 2021), indicative of potential hybridization (*e.g.*, Chang *et al.* 2013; Zhou *et al.* 2017) or allopatric speciation (Kao *et al.* 2019; Wei & Zhang 2022).

Our findings indicate that the difficulties in species delimitation are not isolated but reflect broader ongoing evolutionary processes. Although this study did not aim to provide taxonomic treatment, we emphasize the need for future work with expanded population-level sampling and broader geographic coverage for genomic, spectral, and morphometric data, coupled with ongoing niche investigations (Lima et al. 2025).

These approaches have been fundamental to resolving species complexes in ferns. For example, molecular tools have been essential to unravel cryptic lineages and reticulate evolution in the *Polypodium vulgare* complex (Sigel *et al.* 2014) and have allowed us to trace complex hybridization events and identify cryptic hybrid lineages in the Thelypteridaceae family (Bloesch *et al.* 2022). Furthermore, the combination of genetic data and niche modeling has successfully delineated taxa that exhibited strong morphological overlaps, such as *Lepisorus yamaokae* Seriz. (Fujiwara *et al.* 2022), and adaptive differentiation in *Pteris fauriei* Hieron. (Chao *et al.* 2024). Such tools are crucial because the use of macromorphology only often masks incipient speciation processes, as observed in the *M. piloselloides* complex.

Our results support the recognition of the group comprised of *M. piloselloides*, *M. tobagensis*, and *M. reptans* as a species complex (referred as *M. piloselloides* complex). Although

Microgramma is characterized by high morphological disparity compared to closely related groups, the extensive overlap in phenotypic space observed in this complex may reflect strong conservatism and the retention of ancestral characteristics (Ranker *et al.* 2004; Sundue & Rothfels 2014; He *et al.* 2018). This complex shares highly similar vegetative characteristics, which historically resulted in recurrent descriptions now placed in synonymy (Almeida 2014). The shared phenotypic similarity among these lineages may stem from the retention of plesiomorphic traits, coupled with cross-linking and hybridization events, common phenomena in plant evolution (Chang *et al.* 2013; Liao *et al.* 2015; Zhou *et al.* 2017; Kao *et al.* 2019; Wei & Zhang 2022; Wu *et al.* 2024). Furthermore, other evolutionary processes such as introgression should be considered, where backcrossing of hybrids and parents impacts and increases variability and introduces new genetic characteristics (López-Caamal & Tovar-Sánchez 2014; Suarez-Gonzalez *et al.* 2018). Spectral data (Mendonça *et al.* 2026) corroborate this scenario by presenting cross-error rates between lineages of the *piloselloides* complex, confirming that these overlaps are not methodological artifacts (Slaton *et al.* 2001; Castro-Esau *et al.* 2006; Xiao *et al.* 2016). These species may represent a phenotypic gradient of closely related taxa that are still transiting in the "gray zone" of speciation, an intermediate evolutionary stage of genetic divergence where the separation of lineages occurs gradually and has not yet produced a robust and fixed morphological or chemical differentiation (Roux *et al.* 2016; Sánchez *et al.* 2023).

This scenario of phenotypic overlaps observed in the *M. piloselloides* complex reflects the continuous variation in frond shape, resulting in morphological overlaps, frequently present in ferns, where homoplasy and phenotypic plasticity diminish the diagnostic value of individual characters (Ranker *et al.* 2004; Korall *et al.* 2007; Zhang *et al.* 2017). These and other limitations require the adoption of integrative systematics for this group, which advocates testing specific hypotheses using multiple independent lines of evidence (Dayrat

2005; De Queiroz 2007; Pante *et al.* 2015). Taxonomy based solely on qualitative macromorphological characters has limited effectiveness in species delimitation, particularly for cryptic lineages or any groups where homoplasy and phenotypic plasticity are prevalent (André & Almeida 2025).

The observed patterns, as seen in the *M. piloselloides* complex, are not unique to *Micrograma*; they reflect broader evolutionary dynamics documented in other Polypodiaceae, where homoplasy and adaptive convergence challenge the delimitation of closely related lineages (Lehnert *et al.* 2009; Schneider *et al.* 2009; Labiak *et al.* 2010; Schneider 2016). For example, phylogenetic and morphometric analyses of *Lellingeria* A.R.Sm. & R.C.Moran and the segregated genus *Leucotrichum* Labiak indicate that distinctions based solely on frond or scale characters often do not reflect the true evolutionary history of these species (Labiak *et al.* 2010). Similarly, studies integrating morphology and chloroplastid DNA data have revealed a relatively recent radiation of *Melpomene* A.R.Sm. & R.C.Moran in tropical America, characterized by limited morphological differentiation and pronounced convergence in vegetative characteristics (Lehnert *et al.* 2009). Comparable phenomena have been documented in several other fern lineages (Ranker 2004; Rouhan *et al.* 2004; Schuettpelz *et al.* 2007; Korall 2007; Rothfels *et al.* 2008; Lehtonen *et al.* 2010).

Considering the functional variation of the fronds, we observed that dimorphic species exhibited greater dispersion in multidimensional space and achieved higher classification accuracy (83%) compared to monomorphic lineages (78%; Table 1). This difference in accuracy reflects an evolutionary trade-off between reproduction and survival. Sterile fronds exhibit more conserved forms due to strong selective pressures to maintain maximum photosynthetic function and structural integrity (Vasco *et al.* 2013; Watkins *et al.* 2016). On the other hand, fertile fronds of dimorphic species underwent significant anatomical and evolutionary modifications, which may include narrowing of the blade and rearrangement of

veins specifically shaped to support the energy cost of reproduction and sporangia allocation (Vasco *et al.* 2013). Dimorphism, therefore, can increase the intraspecific variation and increase informativeness in outline analyses. Our morphometric results contrast in part with the results for this same clade using spectral data only, where monomorphic species showed higher prediction rates (Mendonça *et al.* 2026). Since spectroscopy accurately captures the chemical variation present in leaf tissue (Pasquini 2003, 2018; Krähmer *et al.* 2013; Liu *et al.* 2021), the chemical variability introduced between completely distinct and specialized fronds reduces the consistency of the spectral signature, while monomorphic species maintain more homogeneous structural and chemical profiles.

Beyond these phenotypic differences between distinct functional frond types, our comparative phylogenetic analyses provide an additional perspective on the integrated evolution of these characters. By explicitly incorporating evolutionary history through Phylogenetic Generalized Least Squares (PGLS) models, we found that the relationship between frond shape variation and spectra was not statistically significant when each dataset was tested in isolation ($P > 0.05$; Fig. 4). Low λ values in most tests, significant only for combined spectra (Fig. 4C), fertile shape (Fig. 4E) and combined shape (Fig. 4F; Table S3), indicate that the relationship between frond shape and spectra is not strongly structured by phylogenetic relationships. This suggests that covariation between these traits has evolved relatively independently within *Microgramma*, suggesting that changes in frond shape and spectra can respond rapidly to local ecological pressures (Losos 2011), with limited constraint from phylogenetic inheritance (Felsenstein 1985; Revell 2010).

Phylogenetic Partial Least Squares (Phylo-PLS) revealed a significant association between outlines and spectra with all datasets combined. Analyzed separately, however, sterile fronds showed only a moderate association and fertile fronds none (Fig. 5). This result suggests that morpho-spectral integration may depend on the functional state of the frond. Sterile fronds are

mainly associated with light capture and maintenance of water balance, while fertile fronds may be more specialized in reproduction, reflecting distinct selective pressures (Watkins *et al.* 2010; Vasco *et al.* 2013) in the case of dimorphic lineages. Thus, the association detected in the combined set likely reflects the integration of multiple structural and physiological components of the fronds.

This interpretation is consistent with studies demonstrating that leaf spectra are directly related to their anatomical structure, chemical composition, and internal tissue organization (Asner 1998; Jacquemoud & Ustin 2019; Neuwirthová *et al.* 2024), providing reliable signatures for testing taxonomic hypotheses (Mendonça *et al.* 2026). Evolutionary changes in leaf blade architecture can influence how near-infrared radiation interacts with plant tissues, producing distinct spectral signatures among lineages. In epiphytic ferns, where light interception, water retention, and desiccation tolerance are critical ecological factors (Watkins *et al.* 2007; Zotz 2016), small alterations in leaf shape and structure can result in detectable functional differences in both frond shape and spectra (Asner 1998; Jacquemoud & Ustin 2019; Neuwirthová *et al.* 2024).

From a macroevolutionary perspective, the results suggest that the relationship between outlines and spectra in *Microgramma* is characterized by partial phenotypic integration, in which different functional leaf modules can evolve under distinct selective pressures (Pigliucci 2003; Klingenberg 2014). This pattern is consistent with scenarios of modular evolution in plants, in which morphological and physiological characteristics can exhibit different levels of phylogenetic dependence and respond independently to environmental gradients (Ackerly 2004; Losos 2008; Reich 2014). Taken together, our results indicate that the phenotypic diversity observed in the Scaly clade does not result solely from the morphological divergence traditionally used in taxonomy, but also from a complex interaction

between evolutionary history, functional adaptations, and physiological variation detectable by spectroscopy (Cavender-Bares *et al.* 2016; Meireles *et al.* 2020).

CONCLUSIONS

Our results show that variation in frond shape and spectral signatures is informative for delineating species within a phylogenetic context. We demonstrate that these multidimensional traits co-evolve closely with the history of the group. However, far from forming perfectly discrete groups, we quantitatively show that phenotypic variation is largely continuous, resulting in extensive zones of overlap between closely related taxa. It is precisely by translating this complexity into robust quantitative and phylogenetic data that we bridge the gap with the taxonomic challenges of the clade: our results corroborate and expand on the qualitative observations of Almeida (2014). Furthermore, we highlight how an integrative approach can refine the boundaries of species in cryptic groups, overcoming the limitations of single-method analyses. This quantitative framework aligns with a growing trend in plant systematics to interpret morphology as a historical and multidimensional product, rather than merely a collection of diagnostic characters. We emphasize that the precise delimitation of these lineages requires substantially larger sampling, both in terms of individuals and geographic coverage, as well as complementary studies of population genetics and phylogenetic relationships. Only with more comprehensive and homogeneous datasets across the entire distribution of these species will it be possible to reach robust and definitive conclusions about species boundaries. Finally, we believe that the observed morphological overlap between certain lineages should not be considered a methodological artifact, but rather a reflection of the complex biological processes that shape diversity within *Microgramma*. The integration of new lines of evidence and broader sampling represents a promising path to the definitive resolution of these taxonomic uncertainties.

AUTHOR CONTRIBUTIONS

NAM: Conceptualization, Methodology, Investigation, Data curation, Formal analysis, Visualization, Project administration, Writing – original draft. JA: Methodology, Formal analysis, Visualization, Writing – original draft. DVSS: Formal analysis, Writing – review & editing. TEA: Conceptualization, Methodology, Supervision, Writing – review & editing.

ACKNOWLEDGEMENTS

The authors express their gratitude to the Federal University of Pernambuco and to the partner herbaria (BHCB, BR, CEPEC, F, INPA, MEXU, MO, NY, P, RB, UFP, and US). To the technician João Carlos da C. Rangel and the team at the Fuels Laboratory (Institute of Petroleum and Energy Research/UFPE) for their assistance and for providing the spectroscopy equipment. To Drs. Caroline C. Vasconcelos and Bárbara S.S. Leal for their valuable contributions to the manuscript, and to the editors and anonymous reviewers for their feedback, which helped improve this study.

FUNDING INFORMATION

This study was financed in part by the Coordenação de Aperfeiçoamento de Pessoal de Nível Superior—Brasil (CAPES)—Finance Code 001 (88887.132713/2025-00) awarded to NAM, and (88887.132403/2025-00) to DVSS. TEA thanks CNPq for the research grant (317091/2021-2) awarded.

CONFLICT OF INTEREST STATEMENT

The authors declare that there is no conflict of interest.

DATA AVAILABILITY STATEMENT

The raw data, processed data, and R analysis code are publicly available on GitHub: https://github.com/labevofern/Microgramma-Outline.git.

REFERENCES

Ackerly D.D. (2004) Adaptation, Niche Conservatism, and Convergence: Comparative Studies of Leaf Evolution in the California Chaparral. *The American Naturalist*, **163**, 654–671.

Adams D.C., Collyer M.L. (2018) Multivariate Phylogenetic Comparative Methods: Evaluations, Comparisons, and Recommendations. *Systematic Biology*, **67**, 14–31.

Adams D.C., Felice R.N. (2014) Assessing Trait Covariation and Morphological Integration on Phylogenies Using Evolutionary Covariance Matrices. *PLOS ONE*, **9**, e94335.

Adebowale A., Nicholas A., Lamb J., Naidoo Y. (2012) Elliptic Fourier analysis of leaf shape in southern African *Strychnos* section *Densiflorae* (Loganiaceae). *Botanical Journal of the Linnean Society,* **170**, 542–553.

Almeida T.E. (2014) Systematic studies in the genus *Microgramma* C.Presl (Polypodiaceae-Polypodiopsida). Ph.D. Thesis, Universidade Federal de Minas Gerais, Brazil.

Almeida T.E. (2026) *Microgramma* in *Flora and Funga of Brasil*. Jardim Botânico do Rio de Janeiro, Rio de Janeiro, Brazil. https://floradobrasil.jbrj.gov.br/FB91654 (accessed: 15 March 2026).

Almeida T.E., Salino A., Dubuisson J.-Y., Hennequin S. (2021) Insights into long-distance dispersal and ecological and morphological evolution in the fern genus *Microgramma* from phylogenetic inference. *Botanical Journal of the Linnean Society*, **196**, 294–312.

André T., Almeida T.E. (2025) Paths and obstacles to an evidence-based, reproducible, and dynamic Plant Taxonomy. *In SciELO Preprints*. https://doi.org/10.1590/SciELOPreprints.12580

Asner G.P. (1998) Biophysical and Biochemical Sources of Variability in Canopy Reflectance. *Remote Sensing of Environment*, **64**, 234–253.

Bickford D., Lohman D.J., Sodhi N.S., Ng P.K.L., Meier R., Winker K., Ingram K.K., Das I. (2007) Cryptic species as a window on diversity and conservation. *Trends in Ecology & Evolution,* **22**, 148–155.

Bloesch Z., Nauheimer L., Almeida, T.E., Crayn D., Field, A.R. (2022). HybPhaser identifies hybrid evolution in Australian Thelypteridaceae. Molecular *Phylogenetics and Evolution*, **173**, 107526.

Bonhomme V., Picq S., Gaucherel C., Claude J. (2014) Momocs: Outline Analysis Using R. *Journal of Statistical Software,* **56**, 1–24.

Casadei-Ferreira A., Camacho G.P., van de Kamp T., Lattke J.E., Feitosa R.M., Economo E.P. (2025) Evolution and functional implications of stinger shape in ants. *Evolution*, **79**, 80–99.

Castro-Esau K.L., Sánchez-Azofeifa G.A., Rivard B., Wright S.J., Quesada M. (2006) Variability in leaf optical properties of mesoamerican trees and the potential for species classification. *American Journal of Botany*, **93**, 517–530.

Cavender-Bares J., Meireles J.E., Couture J.J., Kaproth M.A., Kingdon C.C., Singh A., Serbin S.P., Center A., Zuniga E., Pilz G., Townsend P.A. (2016) Associations of Leaf Spectra with Genetic and Phylogenetic Variation in Oaks: Prospects for Remote Detection of Biodiversity. *Remote Sensing,* **8***,* 221.

618 Chang Y., Li J., Lu S., Schneider H. (2013) Species diversity and reticulate evolution in the
619 *Asplenium normale* complex (Aspleniaceae) in China and adjacent areas. *Taxon,* **62**, 673–
620 687.

621 Chao Y.S., Yang Y.W., Sheue C.R., Lai I.L. (2024) Niche and phenotypic differentiation in
622 fern hybrid speciation, a case study of *Pteris fauriei* (Pteridaceae). *Annals of Botany*, **134**,
623 71–84.

624 Dayrat B. (2005) Towards integrative taxonomy. *Biological Journal of the Linnean Society*,
625 **85**, 407–417.

626 De Queiroz K. (2007) Species Concepts and Species Delimitation. *Systematic Biology,* **56**,
627 879–886.

628 Denis D.J. (2020) *Univariate, bivariate, and multivariate statistics using R: Quantitative*
629 *tools for data analysis and data science*. John Wiley & Sons, Hoboken, EUA: 366 pp.

630 Felsenstein J. (1985) Confidence Limits on Phylogenies: An Approach Using the Bootstrap.
631 *Evolution*, **39**, 783–791.

632 Forsman A. (2015) Rethinking phenotypic plasticity and its consequences for individuals,
633 populations and species. *Heredity*, **115**, 276–284.

634 Fujiwara T., Egashira T., Gutiérrez-Ortega J.S., Hori K., Ebihara A., Watano Y. (2022)
635 Establishment of an allotetraploid fern species, *Lepisorus yamaokae* Seriz., between two
636 highly niche-differentiated parental species. *American Journal of Botany*, **109**, 1456–1471.

637 Gaem P.H., Andrade A., Mazine F.F., Vicentini A. (2022) Tree species delimitation in
638 tropical forest inventories: Perspectives from a taxonomically challenging case study. *Forest*
639 *Ecology and Management,* **505**, 119900.

640 Greenacre M., Groenen P.J.F., Hastie T., D'Enza A.I., Markos A., Tuzhilina E. (2022)
641 Principal component analysis. *Nature Reviews Methods Primers*, **2**, 1–21.

642 Hastie T., Tibshirani R., Friedman J. (2009) Linear Methods for Classification. In: Hastie T.,
643 Tibshirani R., Friedman J. (Eds), *The Elements of Statistical Learning: Data Mining,*
644 *Inference, and Prediction.* Springer, New York: 101–137.

645 Haufler C.H., Hooper E.A., Therrien J.P. (2000) Modes and mechanisms of speciation in
646 pteridophytes: Implications of contrasting patterns in ferns representing temperate and
647 tropical habitats. *Plant Species Biology*, **15**, 223–236.

648 He L., Schneider H., Hovenkamp P., Marquardt J., Wei R., Wei X., Zhang X., Xiang Q.
649 (2018) A molecular phylogeny of selligueoid ferns (Polypodiaceae): Implications for a
650 natural delimitation despite homoplasy and rapid radiation. *TAXON*, **67**, 237–249.

651 Jacquemoud S., Ustin S. (2019) Leaf optical properties. Cambridge University Press,
652 Cambridge, UK: 566 pp.

653 Kao T.T., Pryer K.M., Freund F.D., Windham M.D., Rothfels C.J. (2019) Low-copy nuclear
654 sequence data confirm complex patterns of farina evolution in notholaenid ferns
655 (Pteridaceae). *Molecular Phylogenetics and Evolution*, **138**, 139–155.

656 Karbstein K., Kösters L., Hodač L., Hofmann M., Hörandl E., Tomasello S., Wagner N.D.,
657 Emerson B.C., Albach D.C., Scheu S., Bradler S., de Vries J., Irisarri I., Li H., Soltis P.,
658 Mäder P., Wäldchen J. (2024) Species delimitation 4.0: integrative taxonomy meets artificial
659 intelligence. *Trends in Ecology & Evolution*, **39**, 771–784.

660 Kessler M., Aros-Mualin D. (2025) The power of independent generations in plants. *New*
661 *Phytologist*, **245**, 440–442.

662 Klingenberg C.P. (2014) Studying morphological integration and modularity at multiple
663 levels: Concepts and analysis. *Philosophical Transactions of the Royal Society B: Biological*
664 *Sciences*, **369**, 20130249.

665 Korall P., Conant D.S., Metzgar J.S., Schneider H., Pryer K.M. (2007) A molecular
666 phylogeny of scaly tree ferns (Cyatheaceae). *American Journal of Botany*, **94**, 873–886.

667 Krähmer A., Gudi G., Weiher N., Gierus M., Schütze W., Schulz H. (2013) Characterization
668 and quantification of secondary metabolite profiles in leaves of red and white clover species
669 by NIR and ATR-IR spectroscopy. *Vibrational Spectroscopy*, **68**, 96–103.

670 Krieg C.P., Chambers S.M. (2022) The ecology and physiology of fern gametophytes: A
671 methodological synthesis. *Applications in Plant Sciences*, **10**, e11464.

672 Labiak P.H., Rouhan G., Sundue M. (2010) Phylogeny and taxonomy of *Leucotrichum*
673 (Polypodiaceae): A new genus of grammitid ferns from the Neotropics. *TAXON*, **59**, 911–
674 921.

675 Lehnert M., Kessler M., Schmidt-Lebuhn A.N., Klimas S.A., Fehlberg S.D., Ranker T.A.
676 (2009) Phylogeny of the fern genus *Melpomene* (Polypodiaceae) inferred from morphology
677 and chloroplast DNA analysis. *Systematic Botany*, **34**, 17–27.

678 Liao R.-L., Ma Y.-P., Gong W.-C., Chen G., Sun W.-B., Zhou R.-C., Marczewski T. (2015)
679 Natural hybridization and asymmetric introgression at the distribution margin of two
680 *Buddleja* species with a large overlap. *BMC Plant Biology*, **15**, 146.

681 Lima K.S., Lima L.V., Almeida T.E. (2025) Fantastic plants and where to find them: niche
682 occupancy analysis in neotropical epiphytic species. *In SciELO Preprints*.
683 https://doi.org/10.1590/SciELOPreprints.11070

684 Liu J., Sun Y., Liu W., Tan Z., Jiang J., Li Y. (2021) Association of spectroscopically
685 determined leaf nutrition related traits and breeding selection in Sassafras tzumu. *Plant*
686 *Methods,* **17**, 33.

687 Liu Z.-P. (2013) Linear Discriminant Analysis. In: Dubitzky W., Wolkenhauer O., Cho K.-
688 H., Yokota H. (Eds), *Encyclopedia of Systems Biology*. Springer, New York: 1132–1133.

689 López-Caamal A., Tovar-Sánchez E. (2014) Genetic, morphological, and chemical patterns
690 of plant hybridization. *Revista Chilena de Historia Natural*, **87**, 16.

691 Losos J.B. (2008) Phylogenetic niche conservatism, phylogenetic signal and the relationship
692 between phylogenetic relatedness and ecological similarity among species. *Ecology Letters*,
693 **11**, 995–1003.

694 Losos J.B. (2011) Convergence, adaptation, and constraint. *Evolution*, **65**, 1827–1840.

695 Ma X.H., Chen Z.G., Liu J.M. (2024) Wavelength selection method for near-infrared
696 spectroscopy based on Max-Relevance Min-Redundancy. *Spectrochimica Acta Part A:*
697 *Molecular and Biomolecular Spectroscopy,* **310**, 123933.

698 Martins E.P., Hansen T.F. (1997) Phylogenies and the Comparative Method: A General
699 Approach to Incorporating Phylogenetic Information into the Analysis of Interspecific Data.
700 *The American Naturalist*, **149**, 646–667.

701 Meireles J.E., Cavender-Bares J., Townsend P.A., Ustin S., Gamon J.A., Schweiger A.K.,
702 Schaepman M.E., Asner G.P., Martin R.E., Singh A., Schrodt F., Chlus A., O'Meara B.C.
703 (2020) Leaf reflectance spectra capture the evolutionary history of seed plants. *New*
704 *Phytologist*, **228**, 485–493.

705 Mendonça N.A., de Oliveira M.H.V., Almeida T.E. (2026) A comparison of interspecific
706 and intraspecific phenotypic variation in spectral signatures of ferns with robust versus
707 uncertain species boundaries. *Journal of Plant Research*, **139**.

708 Mevik B.-H., Wehrens R. (2007) The pls Package: Principal Component and Partial Least
709 Squares Regression in R. *Journal of Statistical Software*, **18**, 1–23.

710 Mickel J.T., Beitel J.M. (1988) Pteridophyte Flora of Oaxaca, México. *Memoirs of the New*
711 *York Botanical Garden* **46**, 1–568.

712 Mittelheiser L., Lepoint G., Gillet, A., Frédérichv B. (2022) Ecomorphology of six goatfish
713 species (Mullidae) from Toliara Reef, Madagascar. *Environmental Biology Fishes,* **105**,
714 1015–1032.

715 Mondal S., Moktan S. (2022) Micro-morphological characters in Polypodiaceae and its
716 taxonomic significance. *Webbia,* **77**, 285–305.

717 Morilla L.J.G., Manting M.M.E., Demayo C.G. (2017) Intrafamilial pinna shape variations
718 of fern species under family Thelypteridaceae and Nephrolepidaceae using Elliptic Fourier
719 Analysis. *Journal of Informatics and Mathematical Sciences,* **9**, 1087–1093.

720 Nascimento M.G.P., Mayo S.J., de Andrade I.M. (2021) Distinguishing the Brazilian
721 mangrove species *Avicennia germinans* and *A. schaueriana* (Acanthaceae) by elliptic
722 Fourier analysis of leaf shape. *Feddes Repertorium,* **132**, 77–107.

723 Neuwirthová E., Lhotáková Z., Červená L., Lukeš P., Campbell P., Albrechtová J. (2024)
724 Asymmetry of leaf internal structure affects PLSR modelling of anatomical traits using VIS-
725 NIR leaf level spectra. *European Journal of Remote Sensing*, **57**, 2292154.

726 Orme D., Freckleton R., Thomas G., Petzoldt T., Fritz S., Isaac N., Pearse W. (2025) Caper:
727 Comparative Analyses of Phylogenetics and Evolution in R [R package caper version 1.0.4].

728 Padial J.M., Miralles A., la Riva I., Vences M. (2010) The integrative future of taxonomy.
729 *Frontiers in Zoology,* **7**, 16.

730 Pagel M. (1999) Inferring the historical patterns of biological evolution. *Nature*, **401**, 877–
731 884.

732 Pante E., Schoelinck C., Puillandre N. (2015) From Integrative Taxonomy to Species
733 Description: One Step Beyond. *Systematic Biology*, **64**, 152–160.

734 Paradis E., Schliep K. (2019) ape 5.0: an environment for modern phylogenetics and
735 evolutionary analyses in R. *Bioinformatics*, **35**, 526–528.

736 Pasquini C. (2003) Near Infrared Spectroscopy: fundamentals, practical aspects and
737 analytical applications. *Journal of the Brazilian Chemical Society*, **14**, 198–219.

738 Pasquini C. (2018) Near infrared spectroscopy: A mature analytical technique with new
739 perspectives – A review. *Analytica Chimica Acta,* **1026**, 8–36.

740 Pease J.B., Brown J.W., Walker J.F., Hinchliff C.E., Smith S.A. (2018) Quartet Sampling
741 distinguishes lack of support from conflicting support in the green plant tree of life.
742 *American Journal of Botany*, **105**, 385–403.

743 Pennell M.W., Eastman J.M., Slater G.J., Brown J.W., Uyeda J.C., FitzJohn R.G., Alfaro
744 M.E., Harmon L.J. (2014) geiger v2.0: an expanded suite of methods for fitting
745 macroevolutionary models to phylogenetic trees. *Bioinformatics,* **30**, 2216–2218.

746 Pigliucci M. (2003) Phenotypic integration: Studying the ecology and evolution of complex
747 phenotypes. *Ecology Letters*, **6**, 265–272.

748 Pinheiro F., Dantas-Queiroz M.V., Palma-Silva C. (2018) Plant Species Complexes as
749 Models to Understand Speciation and Evolution: A Review of South American Studies.
750 *Critical Reviews in Plant Sciences,* **37**, 54–80.

751 R Core Team (2025) R: A language and environment for statistical computing (R
752 Foundation for Statistical Computing, Ed.).

753 Ranker T.A., Smith A.R., Parris B.S., Geiger J.M.O., Haufler C.H., Straub S.C.K.,
754 Schneider H. (2004) Phylogeny and evolution of grammitid ferns (Grammitidaceae): a case
755 of rampant morphological homoplasy. *TAXON*, **53**, 415–428.

756 Reginato M., Michelangeli F.A. (2016) Diversity and constraints in the floral morphological
757 evolution of *Leandra* s.str. (Melastomataceae). *Annals of Botany,* **118**, 445–458.

758 Reich P.B. (2014) The world-wide "fast-slow" plant economics spectrum: A traits manifesto.
759 *Journal of Ecology*, **102**, 275–301.

760 Revell L.J. (2010) Phylogenetic signal and linear regression on species data. *Methods in*
761 *Ecology and Evolution*, **1**, 319–329.

762 Revell L.J. (2012) phytools: an R package for phylogenetic comparative biology (and other
763 things). *Methods in Ecology and Evolution*, **3**, 217–223.

764 Rothfels C.J., Windham M.D., Grusz A.L., Gastony G.J., Pryer K.M. (2008) Toward a
765 monophyletic *Notholaena* (Pteridaceae): Resolving patterns of evolutionary convergence in
766 xeric-adapted ferns. *Taxon*, **57**, 712–724.

767 Rouhan G., Dubuisson J.Y., Rakotondrainibe F., Motley T.J., Mickel J.T., Labat J.N., Moran
768 R.C. (2004) Molecular phylogeny of the fern genus *Elaphoglossum* (Elaphoglossaceae)
769 based on chloroplast non-coding DNA sequences: contributions of species from the Indian
770 Ocean area. *Molecular Phylogenetics and Evolution*, **33**, 745–763.

771 Roux C., Fraïsse C., Romiguier J., Anciaux Y., Galtier N., Bierne N. (2016) Shedding Light
772 on the Grey Zone of Speciation along a Continuum of Genomic Divergence. *PLOS Biology*,
773 **14**, e2000234.

774 Sánchez K.I., Huesa E.G.D., Breitman M.F., Avila L.J., Sites J.W., Morando M. (2023)
775 Complex Patterns of Diversification in the Gray Zone of Speciation: Model-Based
776 Approaches Applied to Patagonian Liolaemid Lizards (Squamata: *Liolaemus kingii* clade).
777 *Systematic Biology,* **72**, 739–752.

778 Satopää V., Albrecht J., Irwin D., Raghavan B. (2011) Finding a “kneedle” in a haystack:
779 Detecting knee points in system behavior. *Proceedings - International Conference on*
780 *Distributed Computing Systems*, **31**, 166–171.

781 Schlick-Steiner B.C., Steiner F.M., Seifert B., Stauffer C., Christian E., Crozier R.H. (2010)
782 Integrative taxonomy: A multisource approach to exploring biodiversity. *Annual Review of*
783 *Entomology,* **55**, 421–438.

784 Schneider H. (2016) Tempo and mode in the evolution of morphological disparity in the
785 Neotropical fern genus *Pleopeltis*. *Biological Journal of the Linnean Society,* **118**, 929–939.

786 Schneider H., Smith A.R., Pryer K.M. (2009) Is morphology really at odds with molecules
787 in estimating fern phylogeny? *Systematic Botany*, **34**, 455–475.

788 Schuettpelz E., Schneider H., Huiet L., Windham M.D., Pryer K.M. (2007) A molecular
789 phylogeny of the fern family Pteridaceae: Assessing overall relationships and the affinities
790 of previously unsampled genera. *Molecular Phylogenetics and Evolution*, **44**, 1172–1185.

791 Sigel E.M., Windham M.D., Haufler C.H., Pryer K.M. (2014) Phylogeny, Divergence Time
792 Estimates, and Phylogeography of the Diploid Species of the *Polypodium vulgare* Complex
793 (Polypodiaceae). *Systematic Botany*, **39**, 1042–1055.

794 Slaton M.R., Hunt E.R., Smith W.K. (2001) Estimating near-infrared leaf reflectance from
795 leaf structural characteristics. *American Journal of Botany,* **88**, 278–284.

796 Speed M.P., Arbuckle K. (2016) Quantification provides a conceptual basis for convergent
797 evolution. *Biological Reviews,* **92**, 815–829.

798 Struck T.H., Feder J.L., Bendiksby M., Birkeland S., Cerca J., Gusarov V.I., Kistenich S.,
799 Larsson K.-H., Liow L.H., Nowak M.D., Stedje B., Bachmann L., Dimitrov D. (2018)
800 Finding Evolutionary Processes Hidden in Cryptic Species. *Trends in Ecology & Evolution,*
801 **33**, 153–163.

802 Suarez-Gonzalez A., Lexer C., Cronk Q.C.B. (2018) Adaptive introgression: a plant
803 perspective. *Biology Letters*, **14**, 20170688.

804 Sundue M.A., Rothfels C.J. (2014) Stasis and convergence characterize morphological
805 evolution in eupolypod II ferns. *Annals of Botany,* **113**, 35–54.

806 Taylor, S. A., & Larson, E. L. (2019). Insights from genomes into the evolutionary
807 importance and prevalence of hybridization in nature. *Nature Ecology & Evolution,* **3**, 170–
808 177.

809 Vasco A., Moran R.C., Ambrose B.A. (2013) The evolution, morphology, and development
810 of fern leaves. *Frontiers in Plant Science,* **4**, 345.

811 Viscosi V., Fortini P. (2011) Leaf shape variation and differentiation in three sympatric
812 white oak species revealed by elliptic Fourier analysis. *Nordic Journal of Botany,* **29**, 632–
813 640.

814 Watkins J.E., Churchill A.C., Holbrook N.M. (2016) A site for sori: Ecophysiology of
815 fertile-sterile leaf dimorphy in ferns. *American Journal of Botany,* **103**, 845–855.

816 Wei R., Zhang X.C. (2022) A revised subfamilial classification of Polypodiaceae based on
817 plastome, nuclear ribosomal, and morphological evidence. *TAXON,* **71**, 288–306.

818 Wiens J.J. (2007) Species Delimitation: New Approaches for Discovering Diversity.
819 *Systematic Biology*, **56**, 875–878.

820 Wishkerman A., Hamilton P.B. (2018) Shape outline extraction software (DiaOutline) for
821 elliptic Fourier analysis application in morphometric studies. *Applications in Plant Sciences,*
822 **6**, e01204.

823 Wood T.E., Takebayashi N., Barker M.S., Mayrose I., Greenspoon P.B., Rieseberg L.H.
824 (2009) The frequency of polyploid speciation in vascular plants. *Proceedings of the National*
825 *Academy of Sciences of the United States of America,* **106**, 13875–13879.

826 Xiao Y., Tholen D., Zhu X.G. (2016) The influence of leaf anatomy on the internal light
827 environment and photosynthetic electron transport rate: exploration with a new leaf ray
828 tracing model. *Journal of Experimental Botany,* **67**, 6021–6035.

829 Zhang L., Zhou X.M., Chen D.K., Schuettpelz E., Knapp R., Lu N.T., Luong T.T., Dang
830 M.T., Duan Y.F., He H., Gao X.F., Zhang L.B. (2017) A global phylogeny of the fern genus
831 *Tectaria* (Tectariaceae: Polypodiales) based on plastid and nuclear markers identifies major
832 evolutionary lineages and suggests repeated evolution of free venation from anastomosing
833 venation. *Molecular Phylogenetics and Evolution,* **114**, 295–333.

834 Zhou X.M., Zhang L., Chen C.W., Li C.X., Huang Y.M., Chen D.K., Lu N.T., Cicuzza D.,
835 Knapp R., Luong T.T., Nitta J.H., Gao X.F., Zhang L.B. (2017) A plastid phylogeny and
836 character evolution of the Old World fern genus *Pyrrosia* (Polypodiaceae) with the
837 description of a new genus: *Hovenkampia* (Polypodiaceae). *Molecular Phylogenetics and*
838 *Evolution,* **114**, 271–294.

839 Zotz G. (2016) Plants on plants – the biology of vascular epiphytes. Springer, Cham, CH:
840 282 pp.

Table 1. Predictive performance of Linear Discriminant Analysis (LDA) in Elliptic Fourier Analysis (EFA) for classifying eight *Microgramma* species using 6–10 harmonics. Data are organized by different tested datasets (I = sterile fronds, II = fertile fronds, III: combined sterile and fertile fronds). Monomorphic and dimorphic species are listed separately. The columns with bold values correspond to how many harmonics were chosen for each model, considering the highest accuracy values.

Datasets	**Number of tested harmonics**															**Averages**
	Six			**Seven**			**Eight**			**Nine**			**Ten**			
	I	**II**	**III**	**I**	**II**	**III**	**I**	**II**	**III**	**I**	**II**	**III**	**I**	**II**	**III**	
Monomorphic		73%			76%			75%			**78%**			77%		76%
M. dictyophylla	**70%**	64%	63%	61%	**71%**	53%	56%	71%	53%	61%	68%	**60%**	56%	61%	57%	62%
M. latevagans	**25%**	81%	56%	12%	**88%**	75%	19%	81%	69%	19%	87%	**69%**	19%	87%	75%	57%
M. percussa	**68%**	85%	79%	76%	**88%**	85%	76%	82%	85%	72%	79%	**85%**	68%	79%	87%	80%
M. piloselloides	**62%**	45%	65%	55%	**52%**	72%	59%	41%	79%	59%	38%	**79%**	62%	52%	79%	60%
Dimorphic		80%			82%			82%			**83%**			82%		82%
M. reptans	**73%**	73%	76%	76%	**76%**	82%	70%	73%	79%	70%	73%	**82%**	62%	73%	79%	74%
M. nana	**74%**	42%	71%	74%	**42%**	64%	77%	48%	68%	74%	39%	**71%**	68%	48%	68%	62%
M. tecta	**42%**	45%	48%	45%	**45%**	42%	48%	48%	51%	54%	57%	**58%**	51%	54%	54%	49%
M. tobagensis	**69%**	62%	62%	62%	**62%**	62%	69%	62%	62%	69%	69%	**62%**	62%	62%	56%	63%
Overall accuracy	**62%**	61%	66%	60%	**64%**	67%	61%	63%	69%	62%	62%	**72%**	58%	63%	70%	64%

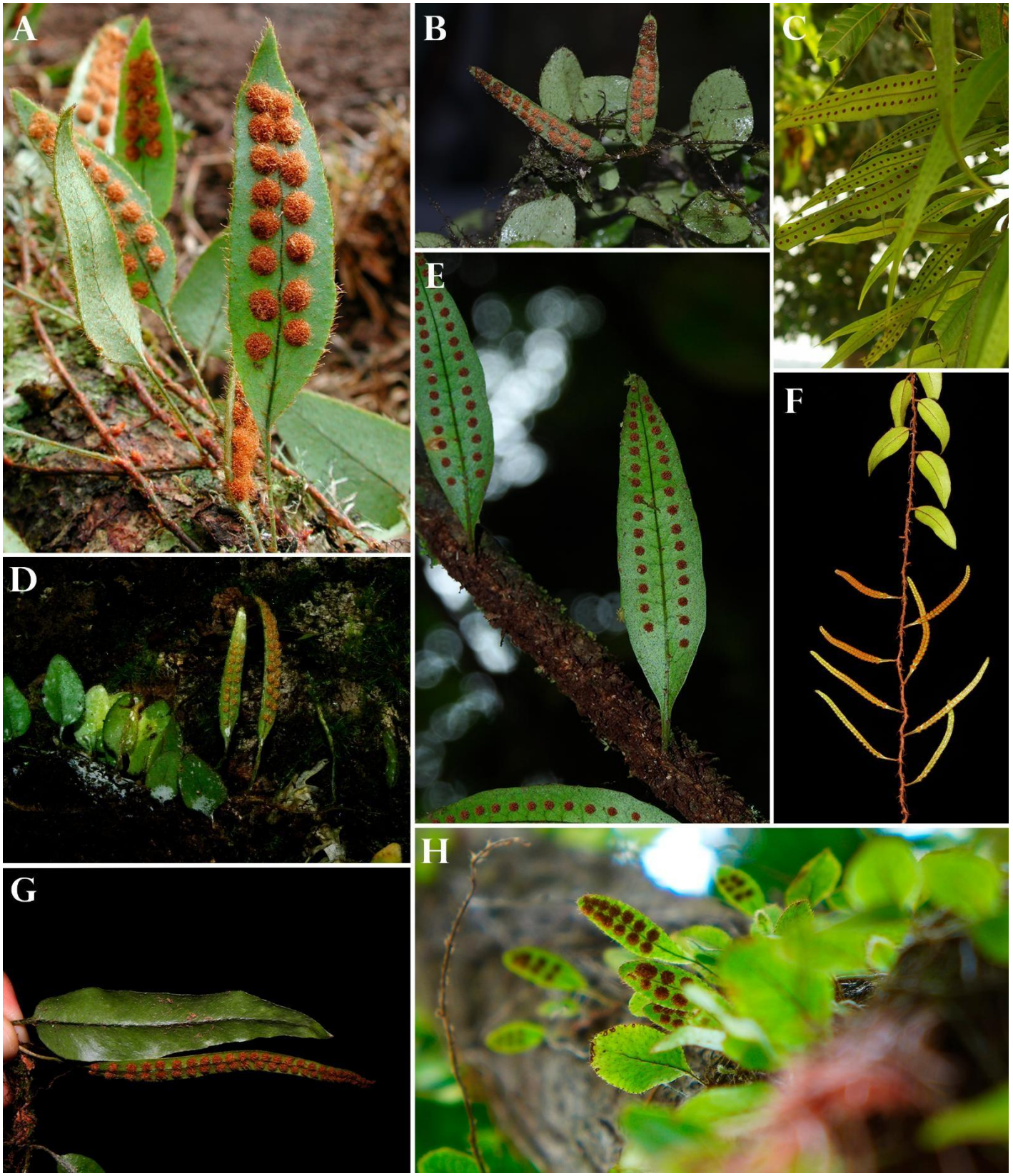

Fig. 1. *Micrograma* species from the Scaly clade. (A) *M. latevagans* (© by 2009 M. Sundue). (B) *M. nana*. (C) *M. percussa*. (D) *M. tecta*. (E) *M. dictyophylla*. (F) *M. reptans*. (G) *M. tobagensis*. (H) *M. piloselloides*.

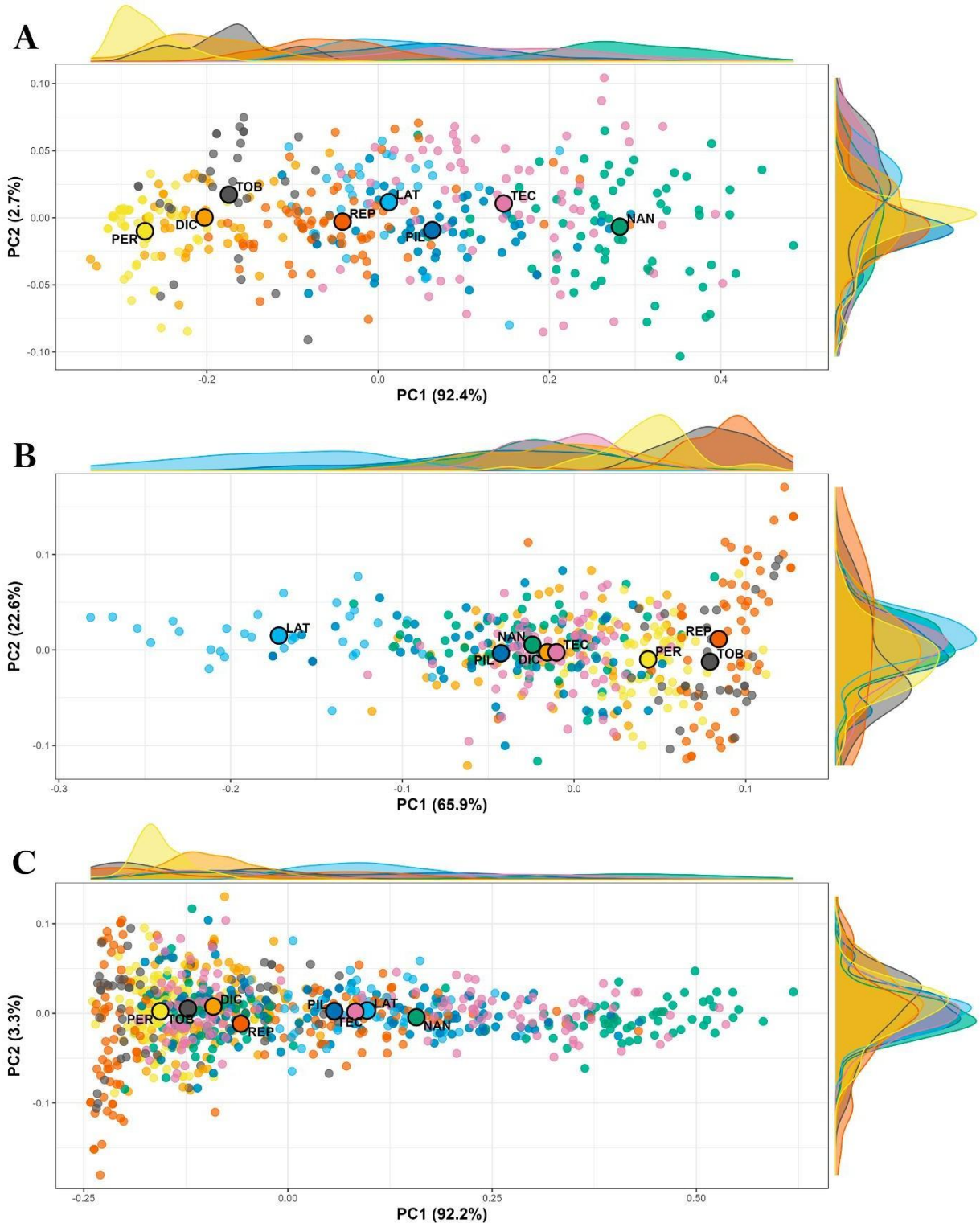

Fig. 2. Principal Component Analysis (PCA) plotted on a two-dimensional graph for sterile, fertile, and combined fronds. The larger circles represent the centroid of each species. (A) PCA of sterile fronds. (B) PCA of fertile fronds. (C) PCA of combined sterile and fertile fronds. DIC=*M. dictyophylla*, LAT=*M. latevagans*, NAN=*M. nana*, PER=*M. percussa*, PIL=*M. piloselloides*, REP=*M. reptans*, TEC=*M. tecta*, and TOB=*M. tobagensis*.

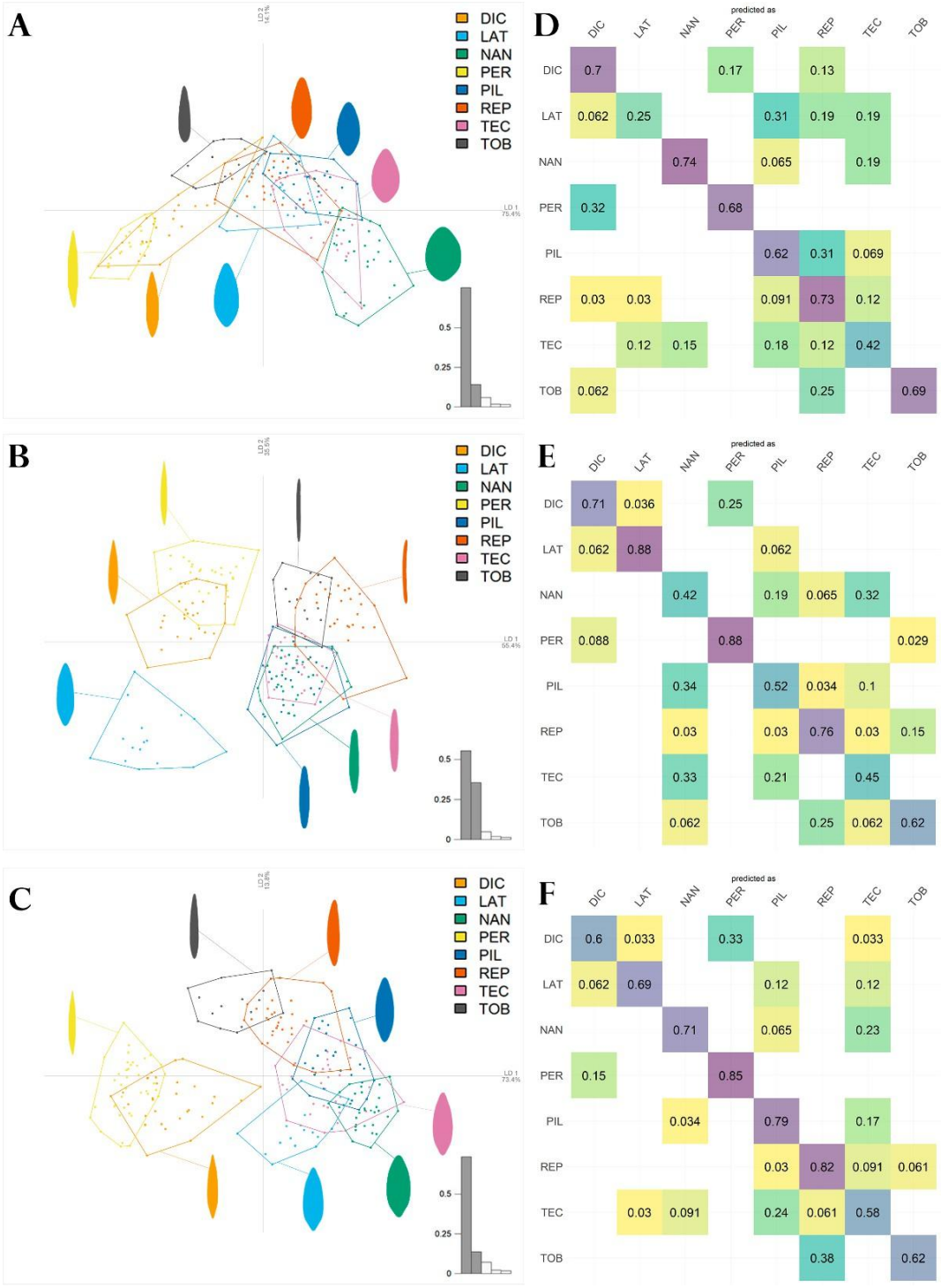

Fig. 3. Linear Discriminant Analysis (LDA) plotted on a two-dimensional graph, with the average shapes of the fronds and the confusion matrices with accuracy values per species for sterile, fertile, and the combined dataset of both fronds. The bar charts in the lower right show the percentage of variance explained by each of the first five PCA axes, ordered from left to right. (A) LDA of sterile fronds. (B) LDA of fertile fronds. (C) LDA of the combined dataset of sterile and fertile fronds. (D) Confusion matrix of sterile fronds. (E) Confusion matrix of fertile fronds. (F) Confusion matrix of the combined dataset of sterile and fertile fronds. DIC=*M. dictyophylla*, LAT=*M. latevagans*, NAN=*M. nana*, PER=*M. percussa*, PIL=*M. piloselloides*, REP=*M. reptans*, TEC=*M. tecta*, and TOB=*M. tobagensis*.

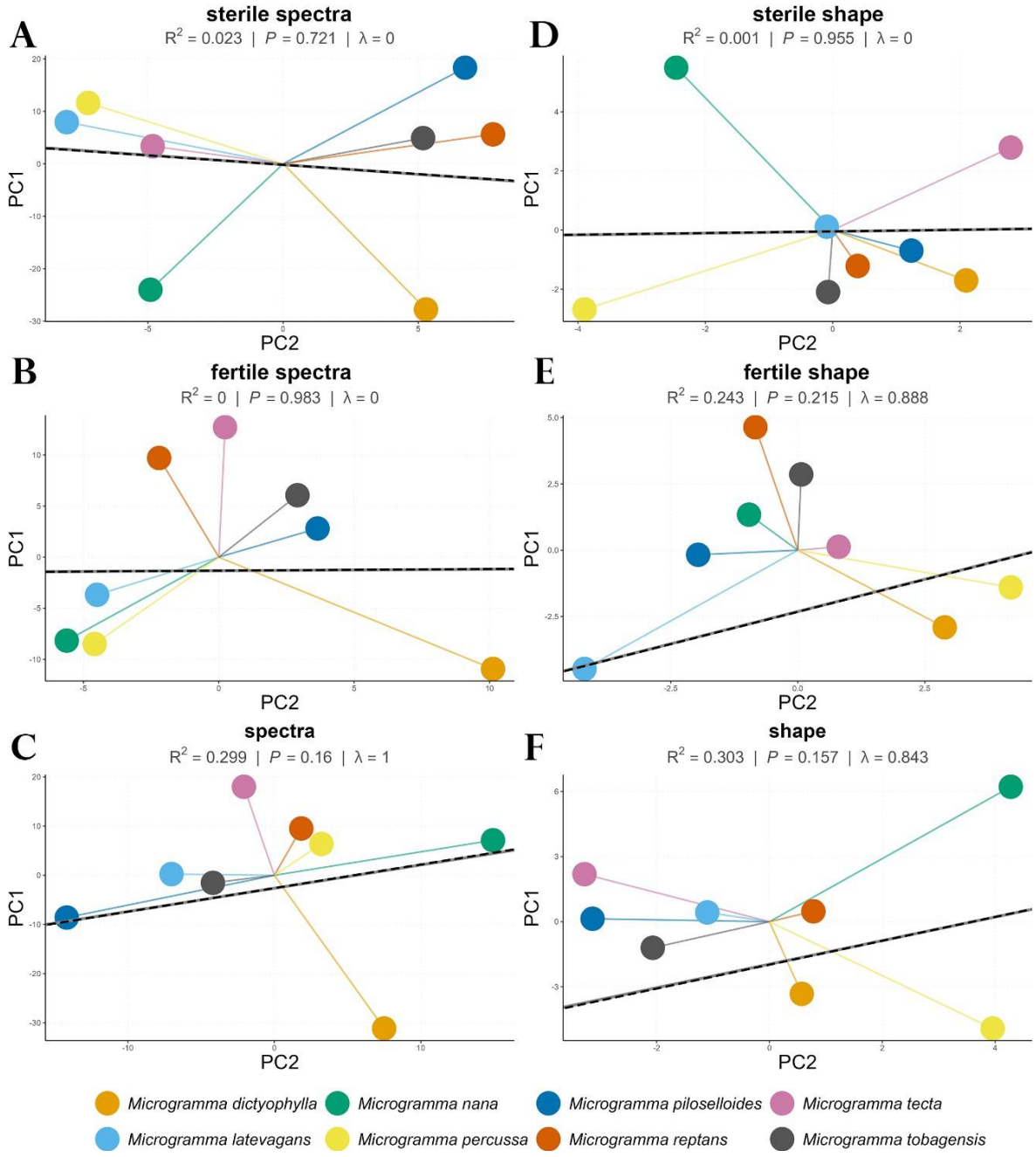

Fig. 4. Phylogenetic Generalized Least Squares (PGLS) regression analyses of morphological and spectral variation for sterile, fertile, and combined datasets. (A) sterile frond spectra (B) fertile frond spectra. (C) combined fertile and sterile fronds spectra. (D) sterile frond shape. (E) fertile frond shape. (F) combined shapes. The R^2 values, *P*-value, and Pagel's lambda (λ) for each dataset are indicated in the subtitle of their respective panels.

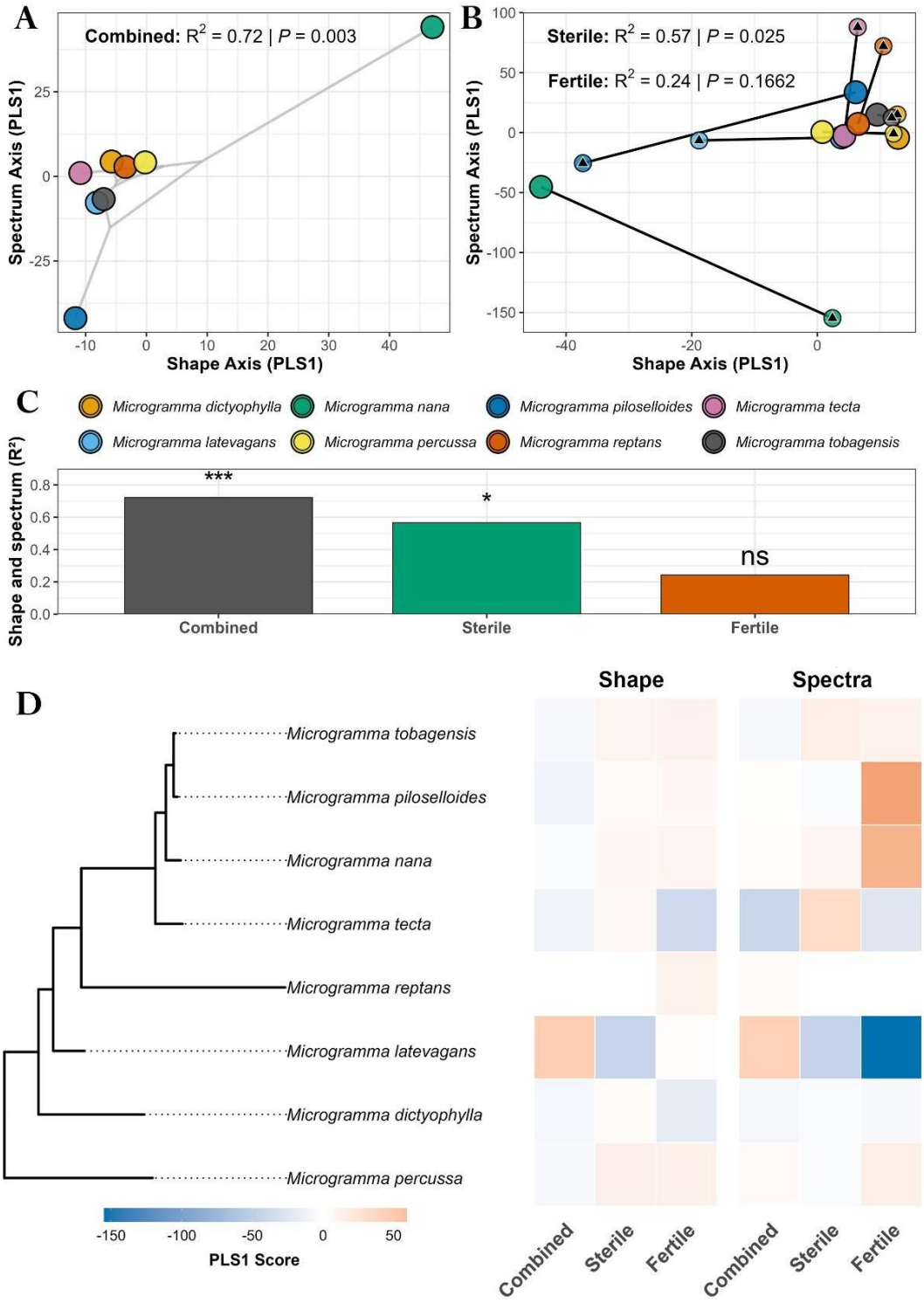

Fig. 5. Analysis of evolutionary integration between frond shape and spectra using Phylogenetic Partial Least Squares (Phylo-PLS) regression. (A-B) Morphospace projected along the phylogenetic relationships in the covariance space between shape (x-axis) and spectra (y-axis). The R^2 values and p-values for each dataset are indicated in the respective panels. (A) Morphospace for the dataset of both sterile and fertile fronds (shape vs. spectra). (B) Morphospace for the dataset of sterile and fertile fronds. The vectors start from the position of the sterile frond (larger circle) and point to the position of the fertile frond (smaller circle with a black triangle). (C) Bar graph comparing the strength of the correlation (R^2) between shape and spectra for the three datasets: combined, sterile only, and fertile only. The

asterisks indicate the level of statistical significance of each correlation (*** $P < 0.001$; ** $P < 0.05$; ns: not significant). (D) Phylogenetic heatmap of PLS1 scores for shape and spectra in the three datasets (Combined, Sterile, and Fertile). The phylogenetic tree (left) shows the evolutionary relationships between species according to Almeida *et al.* (2021). The colors of the tiles represent the magnitude of the PLS1 scores, with a gradient from blue (negative values) to orange (positive values), indicating the direction and intensity of the covariance between shape and spectra in each analysis.

Supplementary Figures and Tables

Title: A multidimensional view of fronds reveals phenotypic structuring and delimitation problems

Authors: Niksoney Azevedo Mendonça[1*], Juliana Aljahara[1], D. Victor Souza e Silva[1] & Thaís Elias Almeida[1]

[1]Programa de Pós-graduação em Biologia Vegetal, Centro de Biociências, Universidade Federal de Pernambuco, Recife–PE, Av. Professor Moraes Rego, 1235, 50670-420, Brazil.

Corresponding author: Niksoney Azevedo Mendonça (Universidade Federal de Pernambuco, Programa de Pós-graduação em Biologia Vegetal).

Phone: +55-98-991213636

E-mail: niksoney.azevedo@ufpe.br

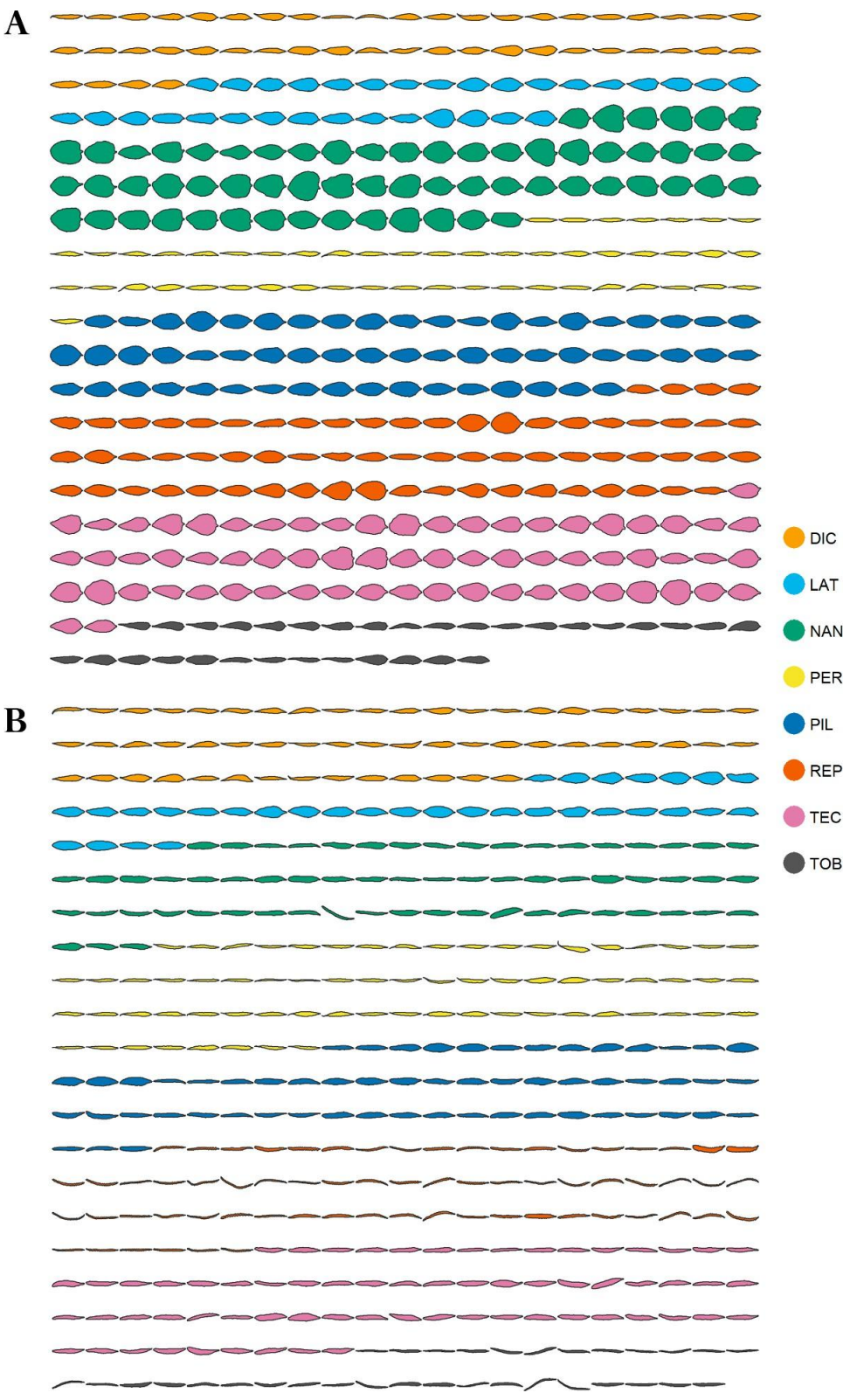

Fig. S1. Variation in the shape of sterile and fertile fronds of eight *Microgramma* species from the Scaly clade (DIC=*M. dictyophylla*, LAT=*M. latevagans*, NAN=*M. nana*, PER=*M. percussa*, PIL=*M. piloselloides*, REP=*M. reptans*, TEC=*M. tecta*, and TOB=*M. tobagensis*). (A) sterile fronds. (B) fertile fronds.

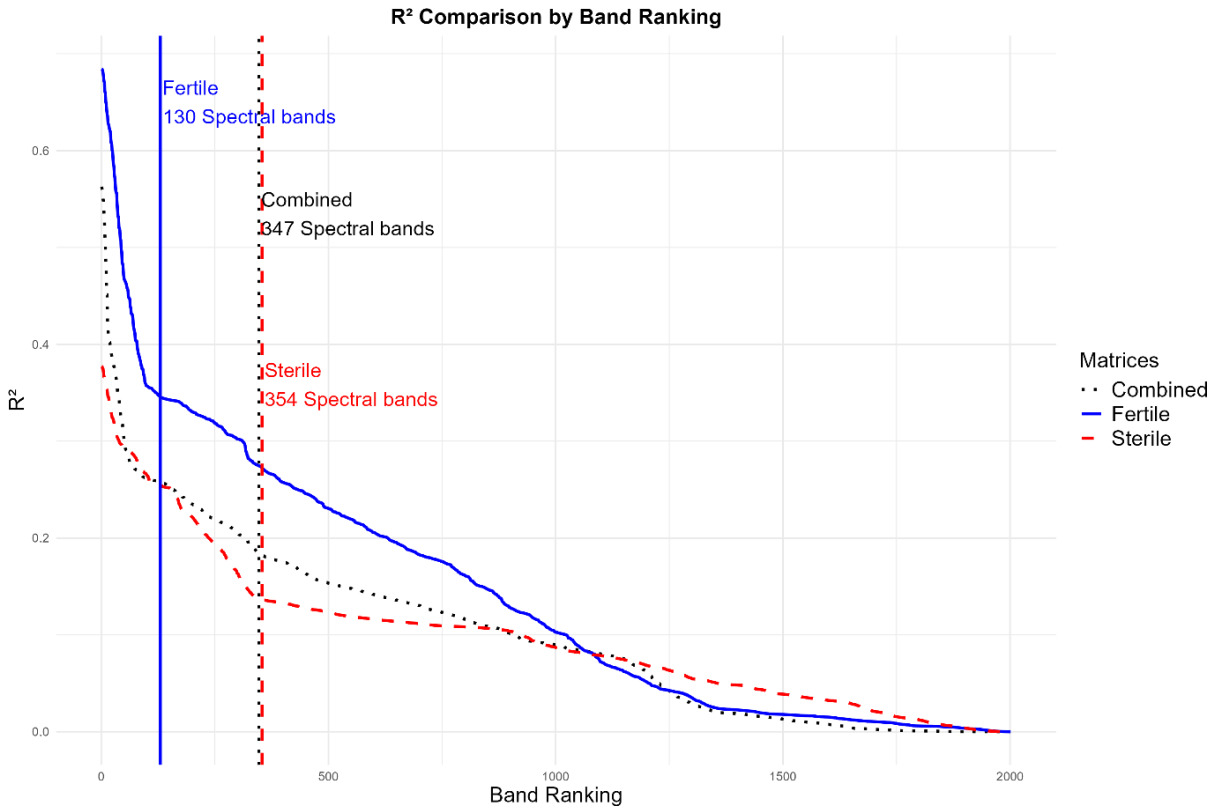

Fig. S2. Selection of spectral bands by maximum relevance for the discrimination of *Microgramma* species. The graph shows the performance of each spectral band, ranked according to its power of discrimination between species, measured by the coefficient of determination (R^2). Three distinct data sets were analyzed: fertile fronds, sterile fronds, and a combined set. The colored vertical lines indicate the “knee point” for each curve, representing the optimal threshold that selects the number of most informative bands, maximizing relevance and minimizing redundancy. The number of spectral bands selected for each dataset is noted on the graph.

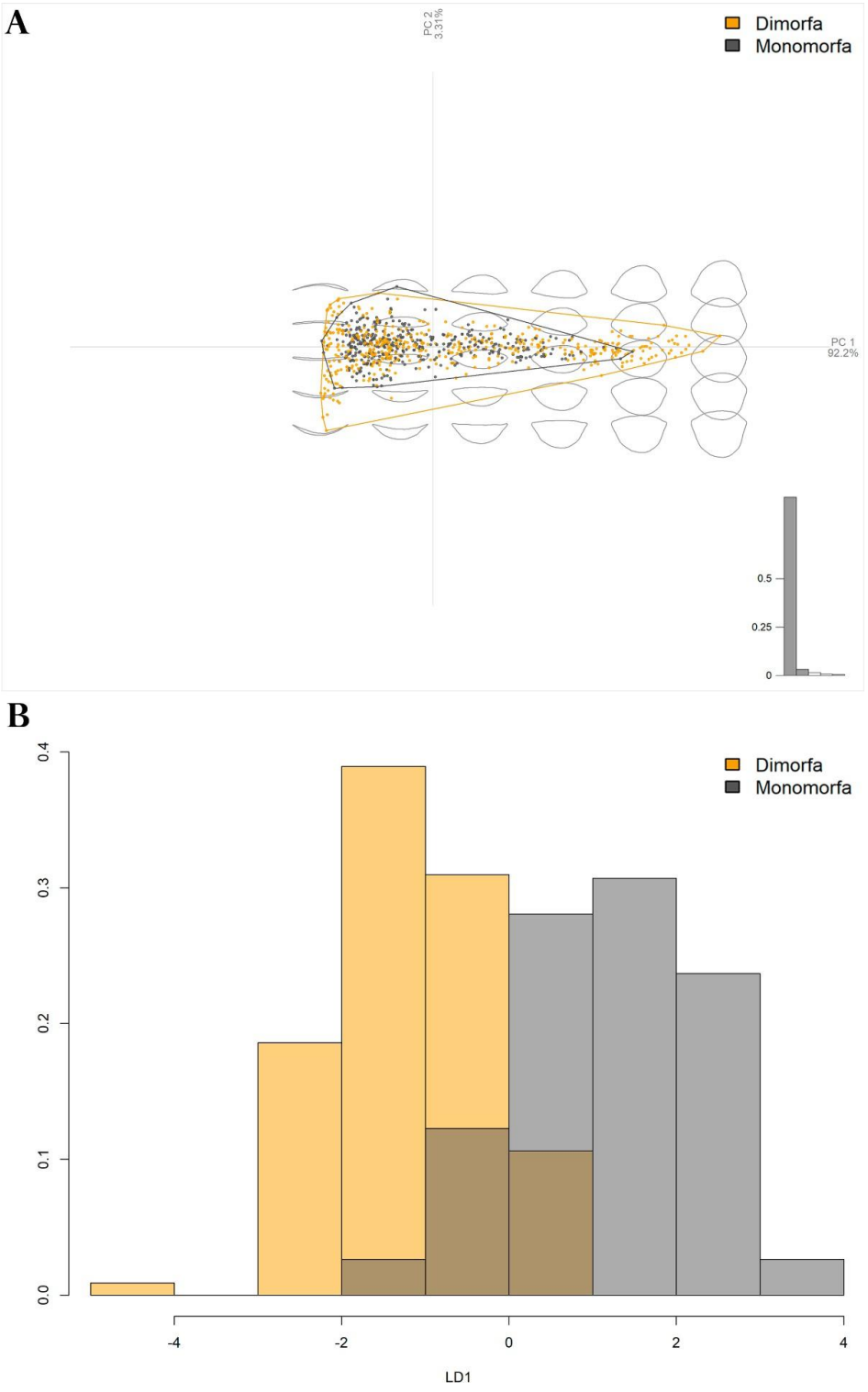

Fig. S3. Principal Component Analysis (PCA) and Linear Discriminant Analysis (LDA) plotted on a two-dimensional graph for dimorphic and monomorphic species. The bar chart in the middle right shows the percentage of variance explained by each of the first three PCA axes, ordered from left to right. (A) PCA of dimorphic and monomorphic species. (B) LDA of dimorphic and monomorphic species.

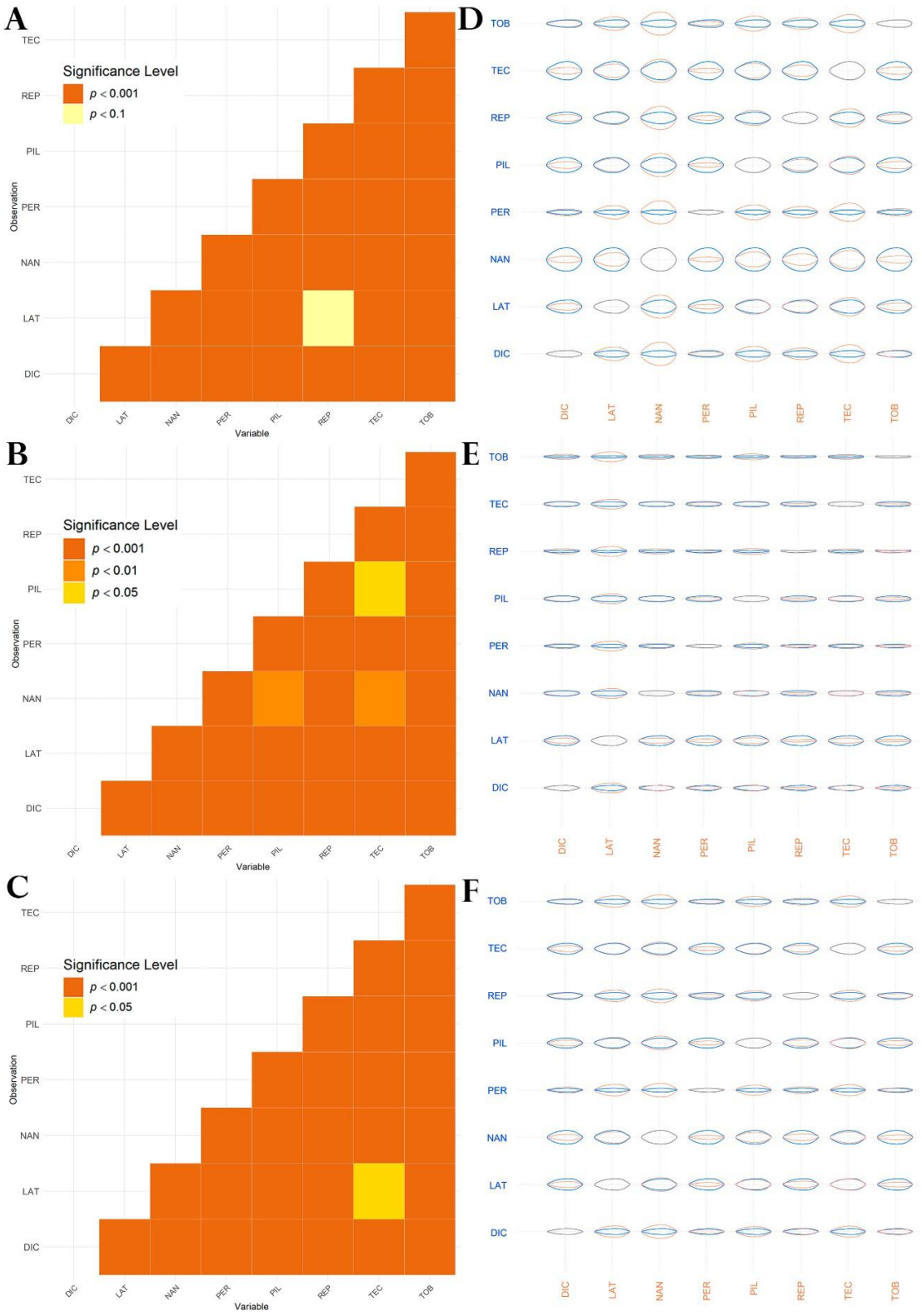

Fig. S4. Multivariate Analysis of Variance (MANOVA) with p-values between the shape of the fronds and the average shape of the species (A) MANOVA of sterile fronds. (B) MANOVA of fertile fronds. (C) MANOVA of combined fronds. (D) mean pair-wise shapes of sterile fronds. (E) mean pair-wise shapes of fertile fronds. (F) mean pair-wise shapes of combined fronds.

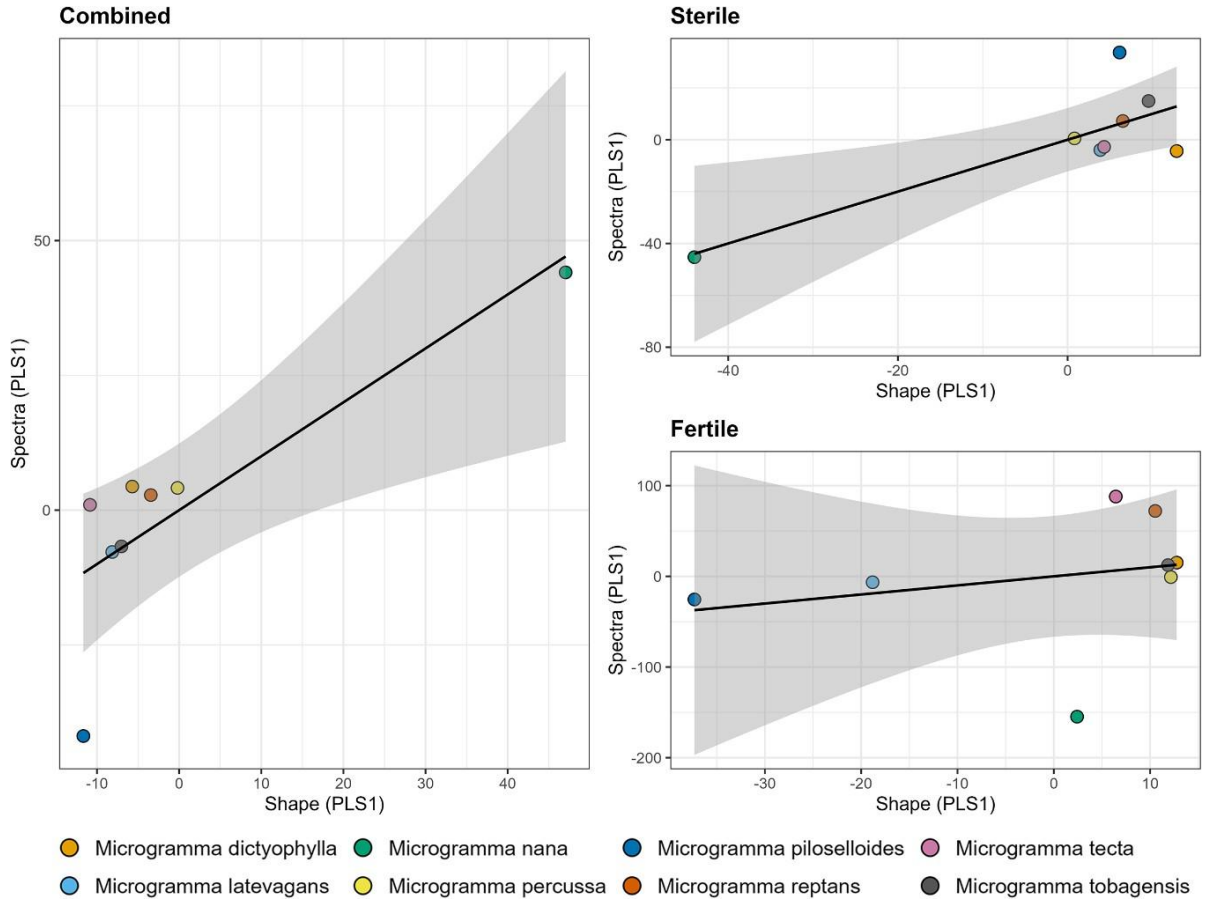

Fig. S5. Relationship between leaf shape and spectral variation in *Microgramma* species. Scatter plots show the regression between the first partial least squares axis of shape (PLS1) and the first partial least squares axis of spectrum (PLS1) for the three datasets (fertile, sterile, and combined). The solid black line indicates linear regression, and the shaded area represents the 95% confidence interval of the model.

Table S1. Specimens used for outline-based geometric morphometrics and spectral data collection. Herbaria abbreviation follows Thiers (2025 continuously updated -https://sweetgum.nybg.org/science/ih/). (*) = specimens used for morphometrics data capture, (**) = specimens used for spectral data readings, (***) = specimens used for both morphometric and spectral data collection.

Species	Country	Voucher
Microgramma dictyophylla	Brazil	Almeida 2230 (BHCB136581) ***
Microgramma dictyophylla	Brazil	Almeida 2605 (BHCB144728) **
Microgramma dictyophylla	Ecuador	Bass 285 (NY03961528) *
Microgramma dictyophylla	Brazil	Berg P18390 (NY00925086) *
Microgramma dictyophylla	Trinidad e Tobago	Broadway 6983 (MO972249) *
Microgramma dictyophylla	Ecuador	Clark 576 (NY03961533) *
Microgramma dictyophylla	Brazil	Cowan 38138 (NY00880067) *
Microgramma dictyophylla	Brazil	Cowan 38507 (NY00880074) ***
Microgramma dictyophylla	Guyana	Cremers 6116 (P01303303) *
Microgramma dictyophylla	Peru	Donald 381 (NY03961555) *
Microgramma dictyophylla	Trinidad e Tobago	Fendler 73 (NY03230423) *
Microgramma dictyophylla	Brazil	Forzza 10340 (RB803843) *
Microgramma dictyophylla	Peru	Foster 7419 (MO3232987) **
Microgramma dictyophylla	Ecuador	Gilmartin 320 (MO1799919) **
Microgramma dictyophylla	Brazil	Granville 12342 (P01352059) *
Microgramma dictyophylla	Guyana	Granville 13521 (P01303310) *

Microgramma dictyophylla	Guyana	Granville 1690 (P01303404) *
Microgramma dictyophylla	French Guiana	Hahn 3679 (P01303402) *
Microgramma dictyophylla	Guyana	Henkel 4933 (NY03961474) *
Microgramma dictyophylla	Venezuela	Liesner 24298 (NY03961515) ***
Microgramma dictyophylla	Suriname	Maguire 39113 (NY03961498) *
Microgramma dictyophylla	Guyana	Maguire 40547 (NY03961499) ***
Microgramma dictyophylla	Guyana	McDowell 4262 (NY03961472) *
Microgramma dictyophylla	Ecuador	Morales 1202 (MO04785303) *
Microgramma dictyophylla	Brazil	Pereira 1095 (RB440043) *
Microgramma dictyophylla	Brazil	Silveira 3976 (RB514332) *
Microgramma dictyophylla	Guyana	Smith 3015 (NY03961496) *
Microgramma dictyophylla	Brazil	Sperling 5901 (NY00880071) *
Microgramma dictyophylla	Peru	Vásquez 21574 (NY03961550) *
Microgramma dictyophylla	Brazil	Vidal 739 (BHCB145204) ***
Microgramma dictyophylla	French Guiana	Werff 12983 (NY03961489) *
Microgramma dictyophylla	Bolivia	Zabalaga MAZ23 (NY03961502) *
Microgramma latevagans	Bolivia	Antezana 1438 (MO04857892) **
Microgramma latevagans	Peru	Bennett 2601 (NY03349971) ***
Microgramma latevagans	Bolivia	Brooke 6661 (NY03961563) *
Microgramma latevagans	Bolivia	Cardenas 1233 (US1742570) *
Microgramma latevagans	Bolivia	Cardenas 3317 (C0653996F) *
Microgramma latevagans	Bolivia	Cayola 1438 (MO04857892) *
Microgramma latevagans	Peru	Diaz s.n. (USM80951) *

Microgramma latevagans	Peru	Dillon 6092 (NY03230430) **
Microgramma latevagans	Bolivia	Herzog 2153 (US01191663) *
Microgramma latevagans	Bolivia	Lewis 881089 (MO4008174) **
Microgramma latevagans	Peru	Quiroz 3396 (C0653990F) *
Microgramma latevagans	Bolivia	Rodriguez 1263 (MO6145673) **
Microgramma latevagans	Peru	Sagástegui 13008 (C0653995F) *
Microgramma latevagans	Peru	Sagástegui 15326 (C0653991F) *
Microgramma latevagans	Peru	Vega 5979 (MO3292118) ***
Microgramma latevagans	Bolivia	Smith 13487 (MO4008613) **
Microgramma latevagans	Bolivia	Smith 1487 (MO4008613) *
Microgramma latevagans	Bolivia	Steinbach 9220 (MO973290) *
Microgramma latevagans	Peru	Vega 5978 (C0653994F) *
Microgramma nana	Brazil	Almeida 2632 (BHCB144755) **
Microgramma nana	Brazil	Almeida 2732 (BHCB149816) ***
Microgramma nana	Bolivia	Altamirano 3649 (MO6184863) *
Microgramma nana	Mexico	Alvaro Campos 1011 (MO05069443) *
Microgramma nana	Ecuador	Asplund 8970 (BR0000032619300) *
Microgramma nana	Ecuador	Aulestia 1192 (MO05045388) *
Microgramma nana	Ecuador	Aulestia 128 (MO6016797) **
Microgramma nana	Colombia	Brant 1697 (MO3516817) *
Microgramma nana	Brazil	Bunbury s.n. (BR0000032619188) *
Microgramma nana	Mexico	Campos 1011 (MO5069443) **
Microgramma nana	Brazil	Carvalho UAT83 (INPA226341) **

Microgramma nana	Ecuador	Croat 59054 (MO3189951) *
Microgramma nana	Ecuador	Croat 86672 (MO6023518) *
Microgramma nana	Venezuela	Davidse 3042 (MO2982712) **
Microgramma nana	Venezuela	Davidse s.n. (MO3484147) *
Microgramma nana	Bolivia	Gentry 70469 (MO4038940) *
Microgramma nana	Brazil	Glaziou 2418 (BR0000032619249) *
Microgramma nana	Costa Rica	Grayum 4884 (MO3324161) **
Microgramma nana	Suriname	Herrera 10088 (MO6069412) ***
Microgramma nana	Ecuador	Holguer 1415 (MO2939704) *
Microgramma nana	Costa Rica	Holm 193 (NY03961398) *
Microgramma nana	Colombia	Idrobo 712 (BR0000032619164) *
Microgramma nana	Panama	Liesner 193 (MO2186491) *
Microgramma nana	Suriname	Maguire 24002 (MO1312664) ***
Microgramma nana	Peru	Monteagudo 16221 (MO6374988) *
Microgramma nana	Peru	Moran 3670 (MO3589534) *
Microgramma nana	Brazil	Mosén 96 (BR0000032619201) *
Microgramma nana	Colombia	Pennell 1586 (MO843969) *
Microgramma nana	Ecuador	Pérez 1185 (NY03962278) **
Microgramma nana	Peru	Revilla 864 (MO2428201) *
Microgramma nana	Brazil	Rocha 341 (RB650639) *
Microgramma nana	Peru	Rojas 649 (MO6102817) *
Microgramma nana	Brazil	Silva 168 (INPA113289) **
Microgramma nana	Peru	Smith 6400 (MEXU644487) *

Microgramma nana	Bolivia	Solomon 17372 (MO3828137) *
Microgramma nana	Venezuela	Steyermark s.n. (MO3098771) *
Microgramma percussa	Colombia	Acosta 1191 (P01281213) *
Microgramma percussa	Nicaragua	Aker 665 (MO5682699) *
Microgramma percussa	Panama	Allen s.n. (MO1176379) *
Microgramma percussa	Brazil	Almeida 372 (BHCB101385) **
Microgramma percussa	Ecuador	Asplund 8568 (BR0000032618372) *
Microgramma percussa	Brazil	Barreto 2595 (BHCB154070) **
Microgramma percussa	Mexico	Breedlove 29899 (MEXU262163) *
Microgramma percussa	Costa Rica	Burger 8904 (MEXU309464) *
Microgramma percussa	Peru	Campos 3991 (MO5302244) **
Microgramma percussa	Colombia	Croat 79621 (MO6027011) **
Microgramma percussa	Belize	Davidse 36445 (MEXU946901) *
Microgramma percussa	Brazil	Dittrich 842 (BHCB64514) **
Microgramma percussa	Brazil	Dusén 15207 (BR0000032618273) *
Microgramma percussa	Brazil	Fraga 3104 (BHCB150254) **
Microgramma percussa	Brazil	Fraga 3176 (RB00618828) *
Microgramma percussa	Brazil	Glaziou 1002 (P01281318) *
Microgramma percussa	Brazil	Glaziou 2387 (BR0000005914456) *
Microgramma percussa	Brazil	Glaziou s.n. (P00625140) *
Microgramma percussa	Belize	Hawkins 1370 (MEXU861143) *
Microgramma percussa	Mexico	Hernández 445 (NY03961228) ***
Microgramma percussa	Panama	Hunter 309 (P01281235) *

Microgramma percussa	Brazil	Jascone 1136 (RB505621) *
Microgramma percussa	Brazil	Labiak 7523 (RB01406780) *
Microgramma percussa	Costa Rica	Lent 2927 (MEXU309446) *
Microgramma percussa	Colombia	Luteyn 10469 (NY03961982) **
Microgramma percussa	Brazil	Madison 618 (INPA85192) **
Microgramma percussa	Mexico	Martínez 15060 (MEXU662973) *
Microgramma percussa	Mexico	Martínez 6370 (MEXU1270610) *
Microgramma percussa	Mexico	Martínez 8601bis (MEXU996003) *
Microgramma percussa	Panama	McDaniel 8077 (MO6576856) ***
Microgramma percussa	Honduras	Molina s.n. (MO2581691) *
Microgramma percussa	Nicaragua	Moreno s.n. (MO3467456) *
Microgramma percussa	Brazil	Nee 7095 (RB224355) *
Microgramma percussa	Honduras	Nelson 7917 (MO3841983) *
Microgramma percussa	Brazil	Ochion s.n. (RB31925) *
Microgramma percussa	Brazil	Pessoa 14 (RB00579845) *
Microgramma percussa	Brazil	Reitz 176 (RB50258) *
Microgramma percussa	Brazil	Salino 1464 (BHCB065966) *
Microgramma percussa	Brazil	Salino 15292 (BHCB066068) *
Microgramma percussa	Brazil	Salino 1988 (BHCB065955) ***
Microgramma percussa	Colombia	Smith 1012 (BR0000032617986) *
Microgramma percussa	Ecuador	Spruce 5242 (P01281121) *
Microgramma percussa	Peru	Sture s.n. (P01281108) *
Microgramma percussa	Bolivia	Windisch 5682 (BHCB061942) *

Microgramma percussa	Brazil	YnesMexia 5118 (P01281383) *
Microgramma percussa	Peru	YnesMexia 6440 (P01607971) *
Microgramma piloselloides	Puerto Rico	Ahlquist 45 (BHCB173388) ***
Microgramma piloselloides	Saint Vincent and the Grenadines	Badger s.n. (MO5484127) **
Microgramma piloselloides	Martinique	Bélanger s.n. (P01281033) *
Microgramma piloselloides	Boneiru	Boom 11057 (NY02099903) **
Microgramma piloselloides	Saint Kitts and Nevis	Britton 166 (NY01842419) *
Microgramma piloselloides	Puerto Rico	Britton 2062 (NY00989767) ***
Microgramma piloselloides	Cuba	Britton 5165 (NY01842276) **
Microgramma piloselloides	Jamaica	Broadway s.n. (MO5446677) ***
Microgramma piloselloides	Cuba	Caluff 1316 (NY01842265) *
Microgramma piloselloides	Dominica	Chambers 2501 (NY01842425) **
Microgramma piloselloides	Jamaica	Clute 248 (P01336509) *
Microgramma piloselloides	Saint Vincent and the Grenadines	Cooley 8474A (NY00674370) *
Microgramma piloselloides	Guadeloupe	Duss 4079 (NY01842416) *
Microgramma piloselloides	Virgin Islands	Eggers 87 (P01336437) *
Microgramma piloselloides	Jamaica	Freed s.n. (MO5462145) *
Microgramma piloselloides	Jamaica	Freed s.n. (MO5462147) *
Microgramma piloselloides	Jamaica	Hitchcock s.n. (MO5446665) **
Microgramma piloselloides	Cuba	Howard 6553 (NY01842286) *
Microgramma piloselloides	Martinique et Guadeloupe	Husnot 370 (P01609476) *
Microgramma piloselloides	Dominican Republic	Liogier 11905 (NY01842351) *
Microgramma piloselloides	Jamaica	Mejía 7508 (MO3859988) **

Microgramma piloselloides	Mexico	Mickel 9054 (NY01842372) *
Microgramma piloselloides	Haiti	Nash 217 (NY01842393) **
Microgramma piloselloides	Jamaica	Riba 113 (MEXU120895) *
Microgramma piloselloides	Jamaica	Riba 115 (MEXU136278) *
Microgramma piloselloides	Costa Rica	Rojas 2067 (MO5900546) ***
Microgramma piloselloides	Jamaica	s.c./s.n. (MO5446680) **
Microgramma piloselloides	Jamaica	s.c./s.n. (MO5462145) **
Microgramma piloselloides	Jamaica	s.c./s.n. (MO5462147) **
Microgramma piloselloides	Guadeloupe	s.c./s.n. (P01336527) *
Microgramma piloselloides	Puerto Rico	Shafer 3139 (NY00989780) **
Microgramma piloselloides	Puerto Rico	Sintenis 1782 (BR0000032618631) *
Microgramma piloselloides	Dominican Republic	Turckheim s.n. (P01336514) *
Microgramma piloselloides	Puerto Rico	Underwood 11 (NY00989773) **
Microgramma piloselloides	Jamaica	Underwood 1368 (NY01842320) *
Microgramma piloselloides	Cuba	Underwood 831 (NY01842269) **
Microgramma piloselloides	Puerto Rico	Vincent 15355 (NY02150502) ***
Microgramma piloselloides	Jamaica	Watt 212 (P01281847) *
Microgramma piloselloides	Dominica	Wilbur 7699 (NY01842412) *
Microgramma piloselloides	Cuba	Wright 798 (BR0000032618570) *
Microgramma piloselloides	Dominican Republic	Zanoni 28119 (NY01842360) ***
Microgramma piloselloides	Haiti	Zanoni 35705 (NY01842381) *
Microgramma reptans	Bolivia	Alice 2366 (MO3783917) *
Microgramma reptans	Ecuador	Aulestia 1560 (MO05055185) ***

Microgramma reptans	Mexico	Breedlove 34129 (MEXU248654) *
Microgramma reptans	Brazil	Daly 1352 (INPA118203) **
Microgramma reptans	Fendler 94	Fendler 94 (BR0000032618822) *
Microgramma reptans	Ecuador	Fierro 2777 (MO5183637) *
Microgramma reptans	Colombia	Fonnegra 1688 (MO3480994) *
Microgramma reptans	Brazil	Forzza 9566 (RB01381733) *
Microgramma reptans	Brazil	Fraga 2971 (RB00596872) ***
Microgramma reptans	Brazil	Fraga 3090 (BHCB150244) **
Microgramma reptans	Brazil	Fraga 3179 (BHCB049785) *
Microgramma reptans	Costa Rica	Gallardo 206 (MEXU976469) *
Microgramma reptans	Brazil	Giacomin 2576 (BHCB191670) *
Microgramma reptans	French Guiana	Granville s.n. (P01280848) *
Microgramma reptans	Guyana	Hoffman 568 (NY03962422) *
Microgramma reptans	Panama	Kennedy 3232 (MO3014609) **
Microgramma reptans	Peru	King 451 (INPA123964) **
Microgramma reptans	Brazil	Labiak 7245 (RB01406938) *
Microgramma reptans	Costa Rica	Lesica 4136 (MO3416567) **
Microgramma reptans	Venezuela	Liesner 6521 (MO2727800) *
Microgramma reptans	Brazil	Maciel 1623 (BHCB065810) *
Microgramma reptans	Suriname	Maguire 25048 (BR0000032618891) *
Microgramma reptans	Mexico	Mares 53 (MEXU695430) *
Microgramma reptans	Brazil	Matos 11468 (CEPEC15838) **
Microgramma reptans	Guyana	MC Dowell 4809 (MO04621215) **

Microgramma reptans	Peru	McDaniel 10931 (RB264198) *
Microgramma reptans	Colombia	Molina 18c716 (MO1626606) **
Microgramma reptans	Ecuador	Palacios 456 (MO3484554) *
Microgramma reptans	Brazil	Pietrobom 8767 (RB760931) *
Microgramma reptans	Guyana	Pipoly 10025 (P01303252) *
Microgramma reptans	Costa Rica	Pittier 9917 (BR0000032618594) *
Microgramma reptans	Peru	Revilla 226 (MEXU521589) *
Microgramma reptans	Bolivia	Rusby 361 (NY03962455) *
Microgramma reptans	French Guiana	Sagot 713 (BR0000032618921) *
Microgramma reptans	Panama	Salino 15879 (BHCB173590) ***
Microgramma reptans	Guyana	sc 7710 (NY03962393) *
Microgramma reptans	Peru	Schunke-Vigo 3469 (INPA133051) **
Microgramma reptans	Panama	Stern 646 (MO1817771) **
Microgramma reptans	Brazil	Torke 2205 (RB01433916) *
Microgramma reptans	Nicaragua	Urbina 70 (MO6710204) **
Microgramma reptans	Suriname	Wullschlägel 669 (BR0000032618839) *
Microgramma tecta	Brazil	Almeida 3203 (BHCB066056) *
Microgramma tecta	Brazil	Bonnet 41027 (RB514349) *
Microgramma tecta	Brazil	Braga 1555 (RB332868) *
Microgramma tecta	Brazil	Braga 2681 (RB466298) *
Microgramma tecta	Brazil	Braga 3428 (RB559156) *
Microgramma tecta	Brazil	Cadorin 1120 (BHCB066044) *
Microgramma tecta	Brazil	Cadorin 2121 (BHCB142972) ***

Microgramma tecta	Brazil	Cadorin 587 (BHCB066016) *
Microgramma tecta	Brazil	Couto 4077 (RB778233) *
Microgramma tecta	Brazil	Daneu 627 (RB566289) *
Microgramma tecta	Brazil	Dittrich 636 (BHCB066031) *
Microgramma tecta	Brazil	Falkenberg 3819 (BHCB061633) *
Microgramma tecta	Brazil	Kaempfe s.n. (RB87297) *
Microgramma tecta	Brazil	Kollmann 4051 (BHCB108513) **
Microgramma tecta	Brazil	Krieger 8862 (BHCB165025) ***
Microgramma tecta	Brazil	Krieger s.n. (BHCB066026) *
Microgramma tecta	Brazil	Labiak 4929 (RB473790) *
Microgramma tecta	Brazil	Labiak 5018 (RB473885) *
Microgramma tecta	Brazil	Labiak 7065 (RB773318) *
Microgramma tecta	Brazil	Lopes 331 (RB375680) *
Microgramma tecta	Brazil	Matos 415 (BHCB97283) ***
Microgramma tecta	Brazil	Mota 3160 (BHCB105182) ***
Microgramma tecta	Brazil	Mota 3670 (BHCB066063) *
Microgramma tecta	Brazil	PaulaSouza 5952 (RB471206) *
Microgramma tecta	Brazil	Salino 10145 (BHCB91558) ***
Microgramma tecta	Brazil	Salino 10917 (BHCB066035) **
Microgramma tecta	Brazil	Salino 13595 (BHCB122753) ***
Microgramma tecta	Brazil	Salino 13779 (BHCB124333) **
Microgramma tecta	Brazil	Salino 4388 (BHCB066066) *
Microgramma tecta	Brazil	Salino 4553 (BHCB066020) *

Microgramma tecta	Brazil	Salino 7495 (BHCB002200) *
Microgramma tecta	Brazil	Salino 8637 (BHCB81163) **
Microgramma tecta	Brazil	Salino s.n. (BHCB43418) **
Microgramma tecta	Brazil	Schmitt 334 (BHCB142994) ***
Microgramma tecta	Brazil	Souza 1195 (BHCB066062) *
Microgramma tecta	Brazil	Souza 1564 (BHCB063026) *
Microgramma tobagensis	Brazil	Amorim 4205 (NY01241079) ***
Microgramma tobagensis	Ecuador	Bass 268 (NY03966125) *
Microgramma tobagensis	Jamaica	Broadway s.n. (NY02027319) **
Microgramma tobagensis	Ecuador	Clark 575 (NY03966129) ***
Microgramma tobagensis	Ecuador	Gudiño 2256 (MO04911176) ***
Microgramma tobagensis	Trinidad e Tobago	Jermy 2680 (MO04642633) ***
Microgramma tobagensis	Trinidad e Tobago	Jermy 2870 (NY02027320) ***
Microgramma tobagensis	Peru	Klug 2539 (NY03966108) **
Microgramma tobagensis	Peru	Knapp 7209 (MO3585354) **
Microgramma tobagensis	Brazil	Matos 1577 (NY02064119) ***
Microgramma tobagensis	Brazil	Mori 11468 (NY01843742) ***
Microgramma tobagensis	Venezuela	Ortega 376 (MO2804046) *
Microgramma tobagensis	Venezuela	Steyermark 61888 (NY03966137) ***
Microgramma tobagensis	Brazil	Thomas 9304 (MO04895073) ***
Microgramma tobagensis	Guatemala	Türckheim 125 (NY03961400) **
Microgramma tobagensis	Ecuador	Vargas 5138 (MO6389474) *
Microgramma tobagensis	Peru	Vargas 7745 (P01280997) *

Microgramma tobagensis	Ecuador	Vargas lópez 5138 (MO6389474) **
Microgramma tobagensis	Peru	Vásquez 31283 (NY03966117) *

Table S2. Multivariate Analysis of Variance (MANOVA) of morphological contours, comparing sterile, fertile, and combined frond models: detailed results and classification proportions. The Hotelling–Lawley trace evaluates the overall multivariate effect between groups; the approximate F value measures the intensity of this effect in relation to the intragroup variance; the degrees of freedom of the numerator and denominator (num Df and den Df) define the distribution of the test; and the *P*-value indicates the probability of observing the effect under the null hypothesis of no difference between groups.

Datasets	**Hotelling-Lawley**	**Approx. F**	**num Df**	**den Df**	***P*-value**
Sterile	6.3743	51.552	49	2774	< 2.2e-16
Fertile	5.5547	30.319	77	2942	< 2.2e-16
Combined	1.4019	20.91	56	5847	< 2.2e-16

Comparison	**Sterile**	**Fertile**	**Combined**
DIC - LAT	1.475e-18	4.364e-25	1.898e-39
DIC - NAN	2.959e-52	6.947e-31	5.374e-36
DIC - PER	1.418e-08	1.125e-12	1.186e-17

Comparison	Sterile	Fertile	Combined
DIC - PIL	6.186e-29	9.166e-31	1.190e-43
DIC - REP	7.516e-20	1.257e-41	3.142e-23
DIC - TEC	6.074e-36	8.863e-33	1.662e-32
DIC - TOB	5.648e-09	7.913e-23	4.630e-26
LAT - NAN	3.227e-21	1.254e-22	7.251e-08
LAT - PER	1.472e-35	5.790e-41	1.758e-74
LAT - PIL	7.590e-04	8.190e-18	3.337e-04
LAT - REP	0.06543	5.255e-42	1.682e-07
LAT - TEC	3.966e-06	1.531e-28	0.01523
LAT - TOB	8.641e-13	4.709e-25	1.093e-23
NAN - PER	1.974e-70	2.182e-40	1.097e-60
NAN - PIL	1.461e-20	0.005272	8.365e-08

Comparison	Sterile	Fertile	Combined
NAN - REP	1.654e-35	4.408e-27	3.927e-11
NAN - TEC	2.922e-09	0.004871	1.075e-05
NAN - TOB	4.120e-42	1.359e-17	1.824e-14
PER - PIL	2.516e-47	2.413e-40	9.360e-67
PER - REP	1.351e-39	9.945e-38	2.735e-40
PER - TEC	1.833e-53	3.411e-41	1.634e-60
PER - TOB	4.049e-22	1.840e-15	2.158e-28
PIL - REP	5.765e-08	5.725e-25	1.021e-07
PIL - TEC	9.128e-07	0.02154	3.335e-05
PIL - TOB	4.674e-20	4.448e-16	1.444e-14
REP - TEC	9.582e-17	9.865e-31	7.767e-06
REP - TOB	2.622e-10	7.440e-06	0.0001084

Comparison	Sterile	Fertile	Combined
TEC - TOB	1.392e-28	2.774e-19	4.458e-10

Table S3. Table S3. Phylogenetically Generalized Least Squares (PGLS) models used to investigate the relationship between the predictor variable PC2 and different phenotypic characteristics (spectra and shape), controlling for evolutionary relationships between species. The residuals (Min, 1Q, Median, 3Q, Max) show the distribution of prediction errors. Likelihood ratio tests [*P*-value ($\lambda = 0$) and *P*-value ($\lambda = 1$)] evaluate whether the phylogenetic signal differs significantly from 0 (no signal) or 1 (Brownian evolution model). The coefficient for PC2 (Est.) shows the magnitude and direction of the predicted effect, with its standard error (SE) indicating the precision of the estimate. The t-statistic and p-value assess the significance of the predictor variable ($P < 0.05$ is considered significant). Model statistics evaluate overall performance: the Residual Standard Error measures the average dispersion around the line of best fit; the adjusted R^2 corrects for the number of parameters and may be negative if the model is inadequate; and the F-statistic evaluates the overall model significance.

Dataset	**sterile spectra**	**sterile shape**	**fertile spectra**	**fertile shape**	**spectra**	**shape**
Residuals						
Min	-186.13	-17.812	-70.81	-19.214	-259.74	-36.058
1Q	-32.91	-12.704	-45.35	-8.704	-57.19	-19.218
Mediana	44.98	-5.244	2.31	-4.141	27.64	7.217
3Q	53.34	5.634	50.32	22.313	60.78	26.324

Dataset	**sterile spectra**	**sterile shape**	**fertile spectra**	**fertile shape**	**spectra**	**shape**
Max	136.75	36.301	90.30	36.561	247.77	35.977
Transformations						
P-value (λ = 0)	1.000	1.000	1.000	0.10608	0.2275	0.37987
P-value (λ = 1)	0.018145	0.0025553	0.12242	0.205	1.000	0.095137
Coefficients						
PC2 (Est.)	-0.36613	0.028519	0.013827	0.48699	0.47340	0.54327
PC2 (SE)	0.97962	0.489346	0.617015	0.35136	0.29568	0.33606
PC2 (t)	-0.3737	0.0583	0.0224	1.3860	1.6010	1.6166
PC2 (*P*)	0.7214	0.9554	0.9828	0.2151	0.1605	0.1571
Statistics						
Residual SE	123.5	19.77	63.67	24.32	159.9	29.45

Dataset	**sterile spectra**	**sterile shape**	**fertile spectra**	**fertile shape**	**spectra**	**shape**
gl residuals	6	6	6	6	6	6
adjusted R^2	-0.1401	-0.166	-0.1666	0.1163	0.1826	0.1873
F-statistics	0.1397	0.003397	0.0005022	1.921	2.563	2.613
gl F	1, 6	1, 6	1, 6	1, 6	1, 6	1, 6

Table S4. Phylogenetic Partial Least Squares (Phylo-PLS) analyses were conducted to evaluate the evolutionary covariation between leaf shape (Shape PCs) and spectral reflectance traits (Spectra PCs) across sterile, fertile, and combined datasets. Comp1 and Comp2 represent the standardized loadings of each variable on the first and second PLS components, respectively, indicating their contribution and direction to the axes of maximal covariation between blocks. The block column identifies whether variables belong to the morphological (Shape) or spectral (Spectra) dataset. Variable Importance in Projection (VIP) scores quantify the relative contribution of morphological predictors to the model, with values > 1 indicating variables of higher importance in explaining the response block. Spectral variables do not present VIP values because they were treated as response variables in the PLS framework. Dataset indicates whether analyses were performed on sterile, fertile, or combined samples.

Variable	Comp1	Comp2	block	VIP	dataset
Shape_PC2	0.54861465	0.72873313	Forma	0.9914685	Sterile
Shape_PC1	-0.85670579	0.6847978	Shape	1.0084594	Sterile
Spectra_PC2	0.56716021	-0.04649469	Spectra	NA	Sterile
Spectra_PC1	0.69043678	0.37257498	Spectra	NA	Sterile
Shape_PC2	0.67293186	0.68028817	Shape	0.9934165	Fertile
Shape_PC1	0.74494625	-0.73294474	Shape	1.0065405	Fertile

Spectra_PC2	0.03787591	0.47846338	Spectra	NA	Fertile
Spectra_PC1	0.16969707	-0.01630461	Spectra	NA	Fertile
Shape_PC2	0.83383492	0.38571235	Shape	0.623725	Combined
Shape_PC1	0.59808298	-0.92261909	Shape	1.2692388	Combined
Spectra_PC2	0.97480877	0.7942833	Spectra	NA	Combined
Spectra_PC1	0.28220454	-0.01676174	Spectra	NA	Combined

Este preprint foi submetido sob as seguintes condições:

- Os autores declaram que os necessários Termos de Consentimento Livre e Esclarecido de participantes ou pacientes na pesquisa foram obtidos e estão descritos no manuscrito, quando aplicável.
- Os autores declaram que a elaboração do manuscrito seguiu as normas éticas de comunicação científica.
- Os autores declaram que estão cientes que são os únicos responsáveis pelo conteúdo do preprint e que o depósito no SciELO Preprints não significa nenhum compromisso de parte do SciELO, exceto sua preservação e disseminação.
- Os autores declaram que os dados, aplicativos e outros conteúdos subjacentes ao manuscrito estão referenciados.
- O manuscrito depositado está no formato PDF.
- Os autores declaram que a pesquisa que deu origem ao manuscrito seguiu as boas práticas éticas e que as necessárias aprovações de comitês de ética de pesquisa, quando aplicável, estão descritas no manuscrito.
- Os autores declaram que uma vez que um manuscrito é postado no servidor SciELO Preprints, o mesmo só poderá ser retirado mediante pedido à Secretaria Editorial do SciELO Preprints, que afixará um aviso de retratação no seu lugar.
- Os autores concordam que o manuscrito aprovado será disponibilizado sob licença Creative Commons CC-BY.
- O autor submissor declara que as contribuições de todos os autores e declaração de conflito de interesses estão incluídas de maneira explícita e em seções específicas do manuscrito.
- Os autores declaram que o manuscrito não foi depositado e/ou disponibilizado previamente em outro servidor de preprints ou publicado em um periódico.
- Caso o manuscrito esteja em processo de avaliação ou sendo preparado para publicação mas ainda não publicado por um periódico, os autores declaram que receberam autorização do periódico para realizar este depósito.
- O autor submissor declara que todos os autores do manuscrito concordam com a submissão ao SciELO Preprints.